We thank the Referee for his/her time and his/her constructive comments. We have complied with most of the proposed changes. In the following, the comments made by the referees appear in black, while our replies are in blue.

1 General Comments

The paper presents a detailed analysis of a case study of ascending motion within the warm conveyor belt region associated with a strong extratropical cyclone in the North Atlantic. The case study occurred during the NAWDEX field campaign which allows for the analysis of rare airborne radar observations with the RASTA system, which is accompanied by online Lagrangian trajectory analysis and a 3D clustering of updraft objects in a convection-permitting simulation. The study, with a strong focus on two individual points in time, confirms recent results from previous case studies that fast ascents can be an integral part of the mostly considered slow and slantwise WCB ascent region. The analysis of online trajectories centered around the RASTA observations and the 3D clustering provide evidence for the occurrence of shallow faster ascents in the cyclone. In particular, the combination of observations, online trajectories and the 3D clustering provide a comprehensive view on fast ascents based on different diagnostics. The occurrence of fast ascents is further divided into different categories of convection, e.g., frontal, banded and mid-level convection. The analysis of fast ascents within the cyclone is complemented by a description of PV evolution along fast and slow ascents and examples of PV distribution associated with rapid ascent. I recommend publication of this manuscript, but I have several major concerns that should be addressed beforehand as well as specific comments and questions listed below:

1. Identification of WCB trajectories
While I agree that the considered case study is indeed a WCB (e.g., Maddison et al., 2019), I do not agree with the here applied identification of individual WCB trajectories with an ascent criterion of 150 hPa in 12 h (l. 106). This performed downscaling of the ascent criterion from the mostly used 500-600 hPa ascent in 48 h (l. 107) captures the mean ascent rate of what is typically considered a WCB, however, it does not ensure that the trajectories actually perform a full ascent from the lower to the upper troposphere. The latter is a defining characteristic of the WCB, as the airstream connects the lower with the upper troposphere (which is correctly mentioned in the introduction). In contrast, the 150 hPa ascent in 12 h, can also include air masses that only rise a little bit but do not perform a substantial cross-isentropic ascent. Indeed, previous studies showed that the WCB airstream is often accompanied by air masses that are only lifted a little (e.g., Wernli et al., 2016; Binder et al., 2020), however, do not themselves define the WCB airstream. I would ask the authors to discuss this topic in section 2.3, and rephrase the sections where the selected trajectories are referred to as 'WCB trajectories' (e.g., l. 136). Please be specific about what is indeed considered as WCB trajectory (i.e., deep cross-isentropic ascent), such as the trajectories per-forming the actual 600 hPa ascent (e.g., l. 173) and what is slow/fast ascent within the overall extended "WCB ascent region" or within the extratropical cyclone (but not necessarily considered a WCB trajectory). In particular, trajectories with fast ascents that remain only in the lower and mid-troposphere should not be considered a WCB trajectory. This is a major concern and should be resolved before publication of the manuscript. To illustrate my point, Fig. 11, for example, shows the ascent of some selected trajectories. The ascent of categories "frontal convection" and "banded convection" appears to flatten out at 3 km height, and hence, would not be considered as WCB trajectory. Instead, it resembles shallow convection in the extratropical cyclone. Finally, the authors themselves mention in the conclusions (l. 441) that WCB trajectories are identified outside of the WCB ascent region, which is contradictory and suggests that the selected trajectories may not all be WCB trajectories: "Contrary to what one might expect, WCB trajectories are identified not only in the WCB ascent region but also in the cloud head and along the warm front of the cyclone". I hence suggest that the authors do not name their selected trajectories per se as 'WCB trajectories' and rephrase the according passages in the manuscript.
We agree with the Referee that the criterion of 150 hPa in 12 h applied here is not equivalent to the usual criterion of 500–600 hPa in 48 h applied in previous studies and is thus not sufficient to define WCB trajectories. This has been clarified in Sect. 2.3, where the criterion is defined: "the 150 hPa threshold

does not ensure that selected trajectories perform a full ascent from the lower to the upper troposphere" and "The selected ascents are thus not all actual WCB trajectories but allow investigating upward motion that would otherwise be excluded with the usual criterion". In addition, identified trajectories that match the criterion are now simply labelled as "ascents" (instead of "WCB ascents"), which remains consistent with their sub-categorization as fast and slow ascents. This has been changed throughout the manuscript, while the term "WCB" has been retained for the more general region of focus. Please note that the few trajectories that actually rise by almost 600 hPa during the 12 h window are not further described, because their number is insignificant (about one hundred out of half a million selected ascents). Futhermore, and as suggested, the time evolution of selected trajectories shown in Fig. 11 is now discussed to distinguish between WCB and other ascents: "These results suggest that trajectories associated with banded and frontal convection at lower levels encounter shallow convection rather than actual WCB ascent. In contrast, trajectories associated with mid-level convection reach typical heights of WCB outflow and thus likely belong to full tropospheric ascents." Finally, the identification of ascents outside the WCB region does not fundamentally contradict the results but the phrasing was unfortunate and has been changed.

2. Trajectory computation
   This point is related to the above comment. Have the authors tried to use a longer time window than 12 h for the trajectory computation? A longer time window (even if some trajectories leave the domain boundary) might allow for a larger number of trajectories that actually perform a WCB-like deep ascent from the lower to the upper troposphere. See also comment to l. 103. Did the authors also consider trajectory computation centered around other times? Do the authors find similar structures and distinction of slow versus fast ascents as for trajectories centered at 16 UTC? How do these structures evolve with time?
   We indeed started with a longer time window for the trajectory computation but later restrained it to 12 h. As mentioned in Sect. 2.3, "This time window is chosen to ensure that trajectories with high wind speed that cross the observation region at 16:00 UTC remain in the simulation domain." This is illustrated in Fig. 4, where many trajectories start close to the southern domain boundary at 10 UTC (red stars) and approach the northern boundary at 22 UTC (brown circles). Increasing the time window might allow for a larger number of deep ascents but also quickly increases the number of incomplete trajectories, which strongly biases the general characteristics described in Sect. 3. This sentence has been added in Sect. 2.3. As for the center of the time window, it is naturally chosen as the time of observations. (Similarly, the center of the simulation domain is chosen as the region of observations.) We have not tried to shift it earlier or later but it does not appear to impact the identification of convective structures, which is based on vertical velocities (instantaneous fields) and rapid segments (2 h periods) and succeeds at highlighting structures at different levels throughout the time window (Figs. 8, 10 and 13). See also Fig. 6, which shows the stability of rapid segments properties with time.

3. RASTA observations
   The study uses rare campaign observations to analyse the radar reflectivity structure of fast ascents in the WCB ascent region. Instead of providing a lengthy comparison of the capability of MESO-NH to simulate the overall radar reflectivity structure (sections 4.1 and 4.3), I would recommend focusing on the region of fast ascents and provide a more detailed analysis and description of the fast ascent regions based on the observational evidence. The availability of such measurements is a great opportunity to obtain more observational evidence of these embedded fast ascents and deserves more detailed consideration.
   Sections 4.1 to 4.3 have been carefully reviewed with particular attention to the size and intensity of convective cells. At the same time, Figs. 7 and 9 have been revised in order to show better the radar observation.

4. Separation of anticyclonic and cyclonic branches
   The performed analysis focuses on the distinction between anticyclonic and cyclonic branches in several sections (e.g., 3.3, 3.4, 3.5). What is the exact reasoning behind the separation into these categories? In Figs. 4, 6 and 11 it appears that the separation is to a large extent determined by the altitude of the trajectories. As expected, trajectories at a higher altitude experience the strong winds from the upper-level jet, and are hence advected anticyclonically. Besides, WCB branches have so far been mostly considered in the upper tropospheric outflow (e.g., Martínez-Alvarado et al., 2014). I am, thus, not

sure if the cyclonic trajectories (which mostly remain below 3-4 km height, e.g., Fig. 4) would be considered a cyclonic WCB branch. Did the authors check, if these trajectories continue their ascent after dt=6 h? Moreover, the separation of "mid-level convection" in cyclonic and anticyclonic subsets (Fig. 12) is not convincing in its current state and additional clarification is needed. Did the authors check if the "cyclonic" trajectories do not turn anticyclonically within the next couple of hours? In the beginning, both clusters overlap, and only at around 20-22 UTC the orange trajectories perform a slight anticyclonic turn. It appears as if the green trajectories could theoretically follow the path of the orange "anticyclonic" trajectories if ex-tended by a few hours. Did the authors consider this possibility? Similarly, the authors define many categories and sub-categories of fast ascents based on the 3D clustering approach. I appreciate that this analysis shows the coherent nature of the individual (shallow) convective regions. Do these categories differ substantially in terms of characteristics and impact? How do these different categories evolve?
The rationale behind the distinction between cyclonic and anticyclonic trajectories is to define contrasting categories in order to better investigate their properties, which is the case for both altitude and location. As noted by the Referee, the separation is to a large extent determined by the altitude, which we believe is an interesting result and appears more elegant than separating the trajectories by altitude in the first place. We thus prefer keeping this categorization for the paper. However, we agree that the contrasting curvatures do not necessarily match the two WCB branches usually defined at the outflow level. We carefully reworded all parts of the paper mentioning cyclonic and anticyclonic trajectories, especially for the former ones, and now mention differences compared to the usual WCB branches: (Section 3.4) "They appear to wrap around the cyclone center and may belong to the cyclonic branch of the WCB, although WCB branches are typically considered at the outflow level (Martínez-Alvarado et al., 2014). The slow ascents located higher in the troposphere (z>8000 m, in orange) take an anticyclonic turn and are located at higher latitudes (above 65° N) at 22:00 UTC, thus are likely part of the anticyclonic branch of the WCB." (This comment is somehow also related to the definition of WCB ascents, see response to major comment 1.) Furthermore, we redesigned Fig. 6 by removing graupel and PV, two variables that did not exhibit much contrast between the categories, and by instead emphasizing rapid segments, which are not diluted in the averaging process. Concerning the evolution of trajectories beyond the study period, we cannot give a definite answer due to biases that would be implied by increasing the time window (see response to major comment 2). Nevertheless, we also agree that trajectories encountering mid-level convection in Fig. 12 are marginally anti/cyclonic only. We thus merged the two subcategories and now discuss their location in light of spatial frequencies for all trajectories in Fig. 5 (see also response to major comment 5).

5. Lagrangian versus Eulerian perspective
In some parts of the study, it is not clearly stated if the Eulerian or the Lagrangian perspective is considered. For example, it is unclear to me if the "WCB frequency" (Figs. 2 and 5) is computed as frequency of trajectories all centered around 16 UTC and following a certain path or if it represents the frequency of the location of trajectory air parcel positions at 16 UTC. The differentiation between this is quite important. If it is the latter, please specify more clearly. "The frequency of trajectories" (l. 137) sounds like it is the first. Please note that a direct comparison of the "trajectory frequency" with Eulerian fields is not valid, as the trajectory frequency spans a 12 h window, while the Eulerian field is only valid at one point in time. See also specific comment to l. 138. In addition, in Figs. 2, 4, and 5 it would be insightful to show the location of the rapid segments which occur at 16 UTC. This would enable a direct comparison of where relative to the fronts the rapid ascent takes place. This type of analysis would complement the 3D object clustering analysis.
Figures 2 and 5 indeed present a Eulerian point of view by displaying spatial frequencies of the identified air parcels at 16:00 UTC, which allow a meaningful comparison with instantaneous fields such as θ_e, while Figs. 4 and 10 present a Lagrangian point of view and thus are carefully not mixed with instantaneous fields. This has been clarified in the text and captions to avoid misunderstandings, e.g., (Fig. 2) "Spatial frequency of air parcels belonging to identified ascents". In addition, as suggested, the three boxes used to define the three categories of convection on Fig. 10b have been added to Fig. 5b and d. This helps comparing (at the very end of Sect. 4) results based on selected trajectories with the general characteristics in Sect. 3.

6. Relation of fast ascents and PV
The PV evolution along trajectories and the discussion section (section 5) about the relation of PV and rapid ascents is in its current form not convincing. I would suggest to either remove these sections or substantially shorten them. In general, I would recommend streamlining the manuscript and focusing on the organization and structure of convective ascents as suggested in the title. The major concerns about the analyses including PV include (i) the robustness and significance of the results with mostly small differences in mean and large interquartile ranges and (ii) the purely descriptive character of the PV signals, i.e., the lack of explanations for the described PV evolution and PV features. See also the specific comments below.
We agree that the relation of PV and rapid ascents is not the core of the paper and that some results may not be significant. However, we believe that the presence of elongated structures of negative PV and their striking similarity with organized convective structures are worth mentioning. Accordingly, Referee 2 asks for more details about the relation between midlevel convection and negative PV features. We thus streamlined the general characteristics of ascents in Section 3 and removed the discussion of PV along fast and slow ascents together with the belonging figure panel. Instead we kept and discussed the clearer time evolution of PV along selected convective ascents in Sect. 4. We also revised the description of PV in cross-sections in Sects. 4 and 5 by carefully avoiding any speculative statements, and added a critical discussion of results in Sect. 6.

2 Specific comments

ABSTRACT

1. l. 8-9: ”The simulation reproduces well the mesoscale structure of the cyclone shown by satellite infrared observations”. This information might not be relevant in the abstract. Removed.
2. l. 9-10: ” the location of trajectories rising by 150 hPa during a relatively short 12h window matches the WCB region expected from high clouds”. This sentence is unclear to me. How do the authors link ascent of 150 hPa with the WCB? It sounds as if the authors identify the WCB from ”high clouds”, however, the WCB is more than just a ”high cloud” layer. The sentence was split and clarified.
3. l. 12: This sentence is a bit confusing. Are the ”convective updrafts” identified directly from the radar or identified in the simulation? Please clarify this sentence. From both; the sentence was clarified.
4. l. 16ff: The presented results about the PV objects and the lower- and upper-level jet are not convincing and very speculative. Please remove this part from the abstract. See also major comment 6 and specific comments below. This part was removed from the abstract.
5. l. 19: The last sentence is repetitive. The last sentence emphasizes the main results of the paper.

1 INTRODUCTION

6. l. 24: The authors could replace ”lower layers of the troposphere” by ”lower troposphere” to streamline the text. Changed.
7. l. 30: See comment to l. 24. The authors could replace ”lower layers of the troposphere” by ”lower troposphere”. Changed.
8. l. 43: What do the authors mean with ”isolated clouds”? If convection is embedded in a larger cloud system such as the WCB as was described, the convective clouds do not appear to be isolated? ”Although convection is usually associated with isolated clouds” has been removed.
9. l. 52: Why also winter, if the field campaign took place in Sep/Oct? Removed.

10. l. 54: Maybe replace ”well sampled” by ”well observed”? Replaced.

11. l. 56: ”More specifically, the onset of a blocking situation over Scandinavia was found unpredictable in the medium-range forecasts.” This information is not relevant at this point. Please explain the relevance for this study in more detail or omit. Removed.

2 DATA and METHODS

12. l. 77: It would help the reader if the authors added the reference directly ”(flight 7of the Falcon 20 aircraft, Schäfler et al. 2018)”. Added.

13. l. 93-96: These sentences are a bit confusing as it is initially unclear, which data comes from the model and which are MSG observations. Please improve this paragraph. Rephrased.

14. l. 100: For simplification, the authors could replace ”the temperature of clouds at their top” by ”cloud top temperature”. Replaced.

15. 15. l. 103: Why did the authors chose a 12-h window? To actually capture WCB trajectories, wouldn’t it be more meaningful to chose a longer time window that would actually capture the WCB ascent from the lower to the upper troposphere with ascent depths that are representative of WCBs (e.g. 500-600 hPa)? See also major comment 1. Did the authors check which percentage of trajectories leaves the simulation domain if the trajectories are actually computed for a longer period? The later mentioned ”banded” and ”frontal” convection do not appear to ascend above 3 km. If these trajectories were run forward for several more hours, would they continue their ascent? See also major comment 2. See response to major comment 2.

16. l. 105 ff: I do not agree with the adapted criterion of 150 hPa ascent in 12 h to identify WCB trajectories. See also major comment 1. ”WCB trajectories” has been changed to ”ascents”. See also response to major comment 1.

17. l. 110 ff: Do the 3D objects need to have a certain size to be identified as a cluster? Could the authors elaborate a bit more on the clustering approach? We added ”Two grid points sharing a common face, either horizontally or vertically, were considered connected, while diagonal connections were considered only vertically. No size criteria were applied”.

18. l. 112: The threshold of 0.3 m s-1 is based on the identification of the so-called ”fast ascents”. Until here, the fast ascents have not been defined. Please add a short explanatory sentence for clarification at this point. The wording ”fast updraft structures” is misleading. It has been changed to ”updraft structures”.

19. l. 112: The applied threshold of 0.3 m s-1 appears low at first sight. The authors could add an estimation of ’typical’ ascent velocities of a WCB (approx. 10 km in 48 h, i.e., ≈0.05 m s-1), which would emphasize the selection of ascent rates that are an order of magnitude larger than what would be expected from the widely-used WCB criterion. The 600 hPa ascent in 12 h discussed in section 3.3 would correspond approximately to such an ascent rate. We added ”This threshold is about five times higher than the typical ascent velocities of a WCB (around 10 km in 48 h, i.e., ≈0.06 m s-1)”.

20. l. 114: Similar to comment above: Do the PV objects need to have a certain size to be considered a cluster? We added ”and without any size criteria.

3 General characteristics of the WCB

21. l. 117: ”is expected to be” sounds vague. Please clarify. Rephrased.

22. l. 118-119: The specification of the colors in brackets is not needed here, because the colorbar in the figure is self explanatory. Removed.

23. l. 120ff: Again "is expected to be" sounds vague. Is the WCB outflow there or not? I find it difficult to distinguish the two branches based on BT alone. How do the authors distinguish that WCB trajectories are ascending into the cloud head? Please make sure to be concise with what is referred to as WCB and how it is identified. Rephrased.

24. l. 112: The authors could add Martínez-Alvarado et al. (2014) as a reference for anticyclonic and cyclonic branches. Added.

25. l. 125: Could the authors describe where the discrepancies in the BT values between MSG and the satellites are found? Changed to "although with larger extent compared against MSG observations".

26. l. 132: "In the simulation, the track shows much more detail with hourly resolution." This is expected in a simulation with higher temporal and spatial resolution. Please streamline this paragraph. Streamlined.

27. l. 137: "The frequency of trajectories fulfilling the WCB criterion of 150 hPa in 12 h". As mentioned before, I don't think the applied criterion is appropriate to identify WCB trajectories. See response to major comment 1.

28. l. 138: "It is integrated on all vertical levels and calculated on coarse meshes of 20 km x 20 km for better visibility." (i) Please specify how it is "calculated" (e.g. interpolated). (ii) Did the authors simply compute the frequency of the Lagrangian trajectories? Or does it show the Eulerian perspective of air parcel trajectory ascent? If it is the first, the "frequency" does not show the actual frequency at 16 UTC, but integrated over the full 12 h window. I.e., it is difficult to combine the Eulerian θe field with the trajectory maxima, because the trajectories at t=-6 h can be located somewhere else relative to the cyclone; similar for the position of trajectories at t=6 h. It could also be meaningful to show the trajectory position at t=0 h (i.e., at 16 UTC). See also major comment 5. See response to major comment 5.

29. l. 138: Please remove "equivalent potential temperature", as it has been introduced before. Removed.

30. l. 143: "Few or no WCB trajectories are detected in the dry intrusion". This is expected, because the dry intrusion is a descending airstream, i.e., dry intrusion and WCB cannot co-occur. Please clarify this part. Clarified.

31. l. 160: For clarification, please include "maximum" pressure variation. Done.

32. l. 173: Although ascent rates of at least 600 hPa in 48 h is often used, previous studies have already shown examples of WCB trajectories that are characterized by faster averaged ascents similar to what is shown in the manuscript (e.g., Fig. 7 in Martínez-Alvarado et al., 2014). We agree. This is stated in the introduction.

33. 33. l. 174: I agree that convective motion can occur for a shorter period of time. However, in particular deep convective motion is often characterized by deep ascents from the lower to the upper troposphere. Do the authors here refer to shallow convection? Can the authors please elaborate and set it into perspective? It has been specified that "fast ascents with a limited total rise likely encounter shallow convection, which will be discussed in the following section". However, please note that both shallow and deep convection are typically intermittent motion compared to continuous slantwise ascent.

34. l. 176: Heading "3.4 Location of slow and fast ascents in the WCB". I suggest to rename the heading to something like "trajectory/path of slow and fast ascents in the WCB", because the evolution of the entire trajectory is shown. Changed to "3.4 Location of slow and fast ascents". Section 3.4 contains two figures: Fig. 4 which shows indeed the complete trajectory of some ascents and Fig. 5 which shows the location of all the ascents at 16:00 UTC.

35. l. 178: Are the selected samples chosen randomly? Are they representative for the entire ensemble of trajectories? We added "randomly selected". Here, these trajectories are shown for overview purpose only. We do not claim that they are representative of all trajectories.

36. l. 178: How do the authors define the "core of the WCB"? While reading the manuscript, I realized that it is explained below (l. 202). Please define it when it is first mentioned. We prefer defining the WCB core later on and changed the wording here.

37. l. 182ff: See general comment 4 for the distinction between anticyclonic and cyclonic trajectories and its dependence on the height level. The belonging to the WCB branches have been carefully reworded, in particular for cyclonic trajectories.

38. l. 187ff: It appears as if the majority of fast ascents starts in the lower troposphere and only reaches 3-5 km height. Did the authors check if these trajectories remain at this elevation or if they continue their ascent? Is this some kind of boundary layer triggered convection? Where relative to the fronts do the rapid segments occur? These questions cannot be answered based on Fig. 4, which is merely a general illustration of the trajectories. The temporal evolution of the ascents is discussed in Sect. 3.5, while the location of rapid segments is assessed in Sect. 4.

39. l. 206: "Fast ascent are mainly located behind the surface cold front and more particularly in its southern part". What do the authors mean with "behind" the cold front? East or west of the front? It is difficult to exactly see the location of the cold and warm fronts in Fig. 5. This could be enhanced by using appropriate colors for the θe-contours or drawing the frontal surfaces. Does Fig. 5 show the frequency of the selected trajectories all centered around 16 UTC or the frequency of air parcel trajectory positions at 16 UTC? See also comment to Fig. 2 and general comment 5. If it shows the frequency of selected trajectories all centered around16 UTC, it is problematic to directly relate it to the position of the fronts, which is a Eulerian field and only valid at 16 UTC. In contrast, the frequency of trajectories would be valid for the full 12 h period. We simplified to "along" the surface cold front and colored θ_e contours as suggested. We also clarified that frequencies relate to "the location of air parcels between slow and fast ascents", i.e., a Eulerian field (see response to general comment 5).

40. l 217: The authors state that the interquartile ranges show a lot of overlap between the fast and slow trajectories and the mean does not differ substantially either. Fig. 6 suggests that there is almost no difference between slow and fast ascents. Does the averaging along trajectories smear out the signal or is there indeed very little difference between the slow and fast ascents? Instead of simply averaging over all the fast and slow ascents, did the authors consider to analyse the rapid segments in more detail? See also comment to l. 353-354. We rewrote the paragraph to emphasize what is clearly different and what is not different between the four categories. We further separated rapid segments between anticyclonic and cyclonic trajectories, which emphasizes that their occur at different altitudes (near 5 and 2 km, respectively), which remain fairly stable during the whole 12 h window.

41. l. 227: The anticyclonic trajectories overlap in altitude (Fig. 6a). But do the corresponding air parcels also overlap in space and time? Fig. 5a,b suggests that there is only partial overlap between fast and slow anticyclonic ascents with the slow ascents mostly north of 60°N and the fast ascents south of 60°N. True. We carefully specified "at least where their location also overlap".

42. l.232: I would have expected the fast ascents to have a larger vertical velocity as the slow ascents. Why isn't this the case? Could the authors go into more detail to further clarify their observations? It was clarified that high values of vertical velocities are diluted in the averaging process, while they are highlighted by showing rapid segments.

43. l. 234: Why did the authors chose to show only graupel mixing ratio, if there is very little graupel actually produced? How about snow and rain? Why is the graupel mixing ratio larger in the slow (cyclonic) ascents than in the fast (cyclonic)ascents? Isn't this counter intuitive? The graupel mixing ratio is now briefly commented only and not shown any more.

44. l. 239-249: The authors discuss the mean evolution of PV values along the different trajectory clusters. What are new insights gained from this analysis? Does the PV structure of the slow and fast ascents differ? It seems as if the PV values are more strongly influenced by the trajectories' height (which is already known, e.g., Wernli et al., 1997; Madonna et al., 2014) than by the distinction between slow versus fast. Please streamline and emphasize what is new. The PV evolution indeed depends on the altitude of

ascents mainly. The figure and description have been removed altogether to keep the PV discussion for Fig. 11, which shows a clearer signal.

4 Fast ascents in the region of observations

45. l. 258: What do the authors mean with "absence of reflectivity values"? Changed to "reflectivites below -20 dBZ".

46. l. 271: I think the authors mean that the black dots show the air parcel positions based on the trajectories, and not the trajectory positions themselves (which would not be a dot only). Are these air parcel positions obtained from the trajectories centered around 16 UTC or did the authors analyse trajectories centered around 15 UTC, too? Changed to "the location at 15:00 UTC of the selected ascents". See also response to major comment 2

47. l. 272-273: In my understanding the dry intrusion is a descending airstream. How can the selected ascending trajectories be located "within the dry intrusion"? Do the authors mean below the dry intrusion? The dry intrusion has been mentioned several times before, how do the authors identify it? See also comment to l. 143. Changed to "below". The dry intrusion is now defined, see response to comment to l. 143.

48. l. 287: What do the authors mean with "topping in the dry intrusion"? Changed to "with cloud tops in the dry intrusion".

49. l. 296-297: Can the authors please elaborate on this? Why would a pressure criterion focus only on lower levels? We added "(a value of 100 hPa $(2h)^{-1}$ is equal to 0.12 m s^{-1} at the surface and 0.3 m s^{-1} at 300 hPa)".

50. l. 297-300: The description about the tropopause and jet structure is a general description of the basic synoptic situation and does not fit in this section about "fast ascents". The description has been reduced to the relevant information here.

51. l. 300ff: Where exactly are the PV dipoles located? The rapid segments are located near a positive PV anomaly (above 2 PVU), but not all rapid segments also coincide with negative PV features (Fig. 8b). In particular, I cannot clearly see dipoles of PV. The description has been simplified to "positive and negative PV structures in the lower and mid troposphere", which are easier to identify.

52. l. 333ff: I am not sure, if I can correctly identify the second cell. Do the authors refer to the rapid segments located at 60°N, too? If yes, could this also be considered as one object or are these clearly separated structures? The two structures are now described together to simplify the discussion.

53. l. 335: I cannot clearly identify the mentioned PV dipole around both convective cells in Fig. 10b. Small-scale negative PV features are present, but where is the positive pole? It seems as if the PV signal is not very pronounced. See also comment to l. 300ff. The description has been simplified as above.

54. l. 337ff: I think that these upper-level convective structures are very interesting, especially because they occur in both the observations and the simulation. Do the authors have any idea why the trajectory analysis does not identify them? Is the rapid ascent in this region too localized or too transient to enable the maintenance of a deep ascent of at least 100 hPa? Do trajectories in this region not meet the ascent criterion of 150 hPa? As explained above, this is due to the identification of fast ascents based on a pressure criterion. It has been clarified in the text.

55. l. 351-353: It appears evident that mid-level convection is located in the middle troposphere. Please streamline. Streamlined.

56. l. 353-354: I find the results in Fig. 11a much more convincing than results in Fig. 6. Did the authors consider streamlining the manuscript and avoid simple averaging over all fast and slow ascents (as in Fig. 6), which does not produce convincing results. Instead, a more detailed analysis of rapid segments would

shed more light into the actual convective ascents. We streamlined the general characteristics Section to focus on convective ascents as suggested. See response to major comment 4.

57. l. 365ff: Can the authors please elaborate on the different PV evolution along the cyclonic and anticyclonic mid-level trajectories (Fig. 11b). What are the mechanisms that lead to these differences? Are these typical characteristics or only valid for trajectories at 16 UTC? Please clarify this part. The figure has changed and cyclonic and anticyclonic mid-level ascents are now merged. Note that we clarified the contrast between frontal and banded convection trajectories vs. midlevel convection trajectories: "This differs from the evolution at low levels, which matches the typical increase below the heating maximum and decrease above (Wernli et al. 1997). Instead, the evolution at mid levels is similar to that found by Oertel et al. (2020) for trajectories passing through a region under convective influence."

58. l. 367: I don't agree that the PV values of all categories are approximately the same in the beginning and end. For example, frontal convection starts with on average ≈0 PVU and ends with ≈1 PVU. Please clarify or avoid this part. This part has been removed.

5 DISCUSSION

59. l. 382-430: Why did the authors choose to name this section "discussion". As this section shows entirely new results and not a discussion of the previous results, I would suggest to rename it accordingly.
I appreciate that the authors show additional times of rapid segments, however, I think that the PV discussion is not yet fully mature and the relation of rapid segments, PV structures, and the low- and upper-level jet is unclear and speculative for the following reasons:
(i) "The results also suggest a link between convection and negative PV production": This appears speculative because negative PV structures frequently occur without rapid segments. Besides, the rapid segments coincide with high positive PV values at 11 and 21 UTC (Fig. 13b,f), while at 16 UTC they coincide with negative PV values (Fig. 13d). Hence, the effect of the rapid segments on PV appears unclear to me;
(ii) "the clustering approach shows that elongated negative PV bands persist for about 10 h": Did the authors track the individual PV bands or PV objects? How did the authors estimate the lifetime of negative PV bands? Are the negative PV bands simply advected or did new PV bands form between the different times?;
(iii) "locally intensify the jet stream": I cannot clearly see this relationship in Fig. 13a,c,e. While in Fig. 13a negative upper-level PV objects indeed coincide with a local jet maximum, this is not the case in Fig. 13c, where distinct negative upper-level PV objects at 61/62°N do not coincide with a local jet maximum. Instead the jet maximum at 9 km height (Fig. 13c) is located in a region where the top altitude of negative PV objects is mostly below 9 km height.
I would kindly ask the authors to clarify the analysis and/or avoid such detailed conclusions.
This section has been revised, as stated in the response to major comment 6, and renamed "Presence of negative PV structures". In particular (i), the possible linkage between convection and negative PV production has been moved to the Conclusions and is now critically discussed based on our results compared to earlier studies: "However, mid-level convective ascents alternatively coincide with positive and negative PV structures, depending on the considered time. Unlike the composite study of Oertel et al. (2019), the formation of horizontal PV dipoles around convective cells thus does not appear systematic, which calls for a more thorough investigation of negative PV formation within WCBs." Concerning the persistence of PV bands (ii), we actually checked the consistency between elongated PV bands at different times by following the corresponding Lagrangian trajectories. However, we do not wish to extend the discussion further with an additional figure and technical details. We thus removed the statement here and now simply state in the Conclusions that the PV bands persist "for several hours", which is easily seen from Fig. 13a and c. Finally (iii), we removed mentions to the possible impact of convection on the low-level and upper-level jets, which are indeed not obvious from the figures.

60. l. 408: "The absence of rapid segments in the negative PV tower at 11:00 UTC suggests that it formed

earlier and upstream". Without more detailed information this statement appears speculative. Please clarify. The statement has been removed.

61. l. 428: "Although a cause and effect relationship cannot be proven, the common shape, location and timing of the identified structures and fast ascents suggest that the organization of negative PV depends on the organization of convection." I do not disagree with this statement, however, I think that the presented results are not yet fully convincing and the conclusions appear rather speculative. Please shorten/remove this discussion about PV. We moved this to the Conclusions, which now critically discuss the production of negative PV.

6 CONCLUSION

62. l. 433: "investigates a possible impact on the associated mesoscale and large-scale dynamics". I think that this aspect is too speculative and contributes only a minor part to the study, and thus, should be avoided in the conclusions. Removed

63. l. 438-439: "thanks to an online tool implemented in the Meso-NH model". This is rather technical and belongs in the methods section. Shortened to "online Lagrangian trajectories".

64. l. 439ff: Please see major comment 1 for my concerns about the WCB trajectory selection. The trajectories are now simply defined as "ascents" in the whole paper.

65. l. 441ff: This is contradictory (see major comment 1) and should be removed. As stated in the response to major comment 1, the phrasing was unfortunate and has been changed.

66. l. 446ff: Please consider the previous comments about the distinction between cyclonic and anticyclonic trajectories and adjust the conclusions accordingly (see major comment 4). The conclusions have been adjusted accordingly.

67. l. 458ff: "Finally, potential vorticity increases along cyclonic ascents – located mainly in the lower troposphere - and decreases along anticyclonic ascents - located mainly in the mid and upper troposphere." Here several aspects are mixed. Are the PV values to a first order determined by cyclonic versus anticyclonic or by low-level versus upper-level? I think it is the latter - please clarify. Besides, is there a clear effect of slow versus fast ascents on PV? Please streamline the conclusions and focus on the main topic of this study, which is organization of convective ascent". PV along fast and slow ascents is not discussed any more. The discussion of PV evolution was then moved to the three categories of convection, which show a clear signal, and updated accordingly.

68. l. 465: "understanding of their formation". How do radar observations provide a better understanding of the formation of fast ascents? I think, they rather provide additional evidence of the existence of fast ascents. As suggested, this was rephrased to radar observations "provide evidence for the existence of fast ascents".

69. l. 476ff: Please streamline this part. In the conclusions it is off little relevance what was not analysed in detail. This part was removed.

70. l.484: "and should therefore have an impact on the upper-level jet stream". I think this is speculative and should therefore be avoided in the conclusions. Removed.

FIGURES

71. Fig. 1: caption: Replace "the position" by "cyclone track" or "evolution of MSLP". Changed to "cyclone track".

72. Fig. 1a: It would be helpful if the authors would also add MSLP and θ_e from the ECMWF analysis in Fig. 1a for comparison with MESO-NH (similar to a comparison of the cyclone track). It might be helpful to color the θ_e contours to better see the fronts. We agree on the interest of showing ECMWF analysis at the time of the MSG observations, that is 16:00 UTC. However, ECMWF does not perform any analysis at that time.

73. Fig. 2: caption: Please rephrase the caption and replace WCB frequency by "frequency of trajectories fullfilling the 150 hPa ascent in 12 h" or similar. See major comment 1. It would be helpful to color the θ_e contours. Besides, is the trajectory frequency shown or the frequency of air parcels at 16 UTC. See also major comment 5. See our response to your major comment 1 regarding the WCB frequency naming. The θ_e contours have been colored.

74. Fig. 3: caption: "WCB trajectories" (see major comment 1). Changed to "ascents" (see response to major comment 1).

75. Fig. 4: It is difficult to see the trajectory locations at the specified times in the figure (in particular the black dots at 16 UTC). Did the authors consider to show the location where the fastest ascent takes place, i.e., the so-called "rapid segments" (location where Δ P(2h)< -100 hPa), too? Especially for the "fast ascents" in the lower troposphere it is difficult to see where the actual ascending motion takes place, as they mostly remain at low levels for the first 6 h (dark blue colors until 16 UTC). These trajectories are randomly selected and shown for overview purpose only. We do not intend to show more details because of their lack of representativeness.

76. Fig. 6: Could the authors please specify what is meant with the following sentence, I am not sure I understand it correctly: "The median and the 25th–75th percentiles for the 2 h rapid segments are shown with boxplots." Did you average over all rapid segments for each hour and regardless of which category they belong to? The anticyclonic slow and fast ascents (Fig. 6b) have very similar median vertical velocities? Is this meaningful? I would expect to see a difference between fast and slow, however, the difference between anticyclonic and cyclonic appears to be larger. Moreover, considering the median evolution of altitude versus time (Fig. 6a), there seems to be little evidence that fast versus slow ascents are characterized by very different averaged ascent behaviour (especially for the anticyclonic trajectories). Figure 6 has been revised. The median and the 25th–75th percentiles for the 2 h rapid segments are now shown separately for slow and fast ascents. The associated text has been revised accordingly.

77. Fig. 7: The presentation of this figure could be improved. In (c,d) the "double hatching for values greater" is hardly visible. In (a,b) instead of using hatching for wind speed, could the authors add colored contours to highlight the region? The trajectory positions are difficult to see. In addition to all WCB air parcel positions, it would be interesting to highlight the location of rapid segments (as in Fig. 8). We improved the readability of Fig 7. In particular, double hatching and yellow contours have been removed in the vertical sections. We did not add the location of rapid segments to keep the figure readable.

78. Fig. 8: This figure is very busy. Could the authors somehow reduce or condense the content shown in the figure? For panel (a) a zoom on the target region where most of the updraft objects are located might improve the visualization. In (b) the grey and light blue contours are very difficult to see in the lower troposphere.Moreover, it is difficult to see the updraft objects, because the many lines cover the shading (e.g. at 23°W). We improved the readability of Fig 8. In particular, light blue contours have been removed in the vertical section and the size and the layout and size of the figures have been modified

79. Fig. 9: See comments to Fig. 7. See response to comments to Fig. 7.

80. Fig. 10: See comments to Fig. 8. See response to comments to Fig. 8.

81. Fig. 12: The following sentence is unclear to me: "Only samples of 10 categories are plotted." Do the authors mean "Only 10 samples of the 4 categories are shown"? Moreover, it would be helpful to show θ_e contours to the see the frontal structure, especially for the category "frontal convection". Changed to "Only 10 samples are shown in each category". We do not show θ_e contours to avoid overlapping trajectories with instantaneous fields (see response to major comment 5).

82. Fig. 13: This figure is very busy and it is difficult to see the individual negative PV objects. Can the authors zoom in and focus on a smaller region? In the regions with many rapid segments the dots sometimes cover the top altitude of negative PV objects. Moreover, I cannot clearly identify the mentioned PV dipoles in panels (b,d,f). We improved the readability of Fig 13.

3 Technical corrections

1. l. 27: Typo: "WVB". Fixed.
2. l. 103: Please replace "centered on the time" by "centered around the time". Done.
3. l. 119-120: The word "troposphere" in "Mid-level troposphere clouds" is not needed. Removed.
4. l. 126: Please add a bracket here: equivalent potential temperature (θ_e). Added.
5. Please replace "convection cells" with "convective cells" and try to be consistent with the wording. It is mixed throughout the text. Similarly, please consistently replace "potential vorticity" by "PV", equivalent potential temperature by θ_e, etc., once it has been introduced. Done.
6. l. 160: What is meant by "upward trajectory"? Do the authors mean upward motion or ascent? Changed to "upward motion".
7. l. 169: I think a "-" is missing in "below-100 hPa 2h-1". Changed to "a pressure variation greater than 100 hPa in 2 h".
8. l. 203: Please add a "s" in "few slow ascent". Done.
9. l. 347: Please be consistent and use "frontal convection". Not changed because these isolated shallow convective cells are not all included in the frontal convection region.
10. l. 351: Please replace "Lagrangian trajectories" by "trajectories". Trajectories are per definition Lagrangian features. Done.
11. l. 456: Please rephrase the following sentence: "during which fast WCB ascents rise above the pressure threshold of 100 hPa (2h)-1". Removed.
12. l. 476: Please replace "several hundred km" by "several hundreds of kilometers". Done.

4 References

Binder, H., M. Boettcher, H. Joos, M. Sprenger, and H. Wernli, 2020: Vertical cloud structure of warm conveyor belts – a comparison and evaluation of ERA5 reanalyses, CloudSat and CALIPSO data. Weather Clim. Dynam. Discussions, 2020, 1–28, doi:10.5194/wcd-2020-26.

Maddison, J. W., S. L. Gray, O. Martiíez-Alvarado, and K. D. Williams, 2019: Upstream Cyclone Influence on the Predictability of Block Onsets over the Euro-Atlantic Region. Mon. Wea. Rev., 147 (4), 1277–1296, doi:10.1175/ MWR-D-18-0226.1.

Madonna, E., H. Wernli, H. Joos, and O. Martius, 2014: Warm conveyor belts in the ERA-Interim dataset (1979-2010). Part I: Climatology and potential vorticity evolution. J. Climate, 27, 3–26, doi:10.1175/JCLI-D-12-00720.1.

Martínez-Alvarado, O., H. Joos, J. Chagnon, M. Boettcher, S. L. Gray, R. S. Plant, J.Methven, and H. Wernli, 2014: The dichotomous structure of the warm conveyor belt. Q. J. R. Meteorol. Soc., 140, 1809–1824, doi:10.1002/ qj.2276.

Wernli, H., M. Boettcher, H. Joos, A. K. Miltenberger, and P. Spichtinger, 2016:A trajectory-based classification of ERA-Interim ice clouds in the region of the North Atlantic storm track. Geophys. Res. Letters, 43, 6657–6664, doi:10.1002/2016GL068922.

Wernli, H., and H. C. Davies, 1997: A Lagrangian-based analysis of extratropical cyclones. I: The method and some applications. Q. J. R. Meteor. Soc., 123, 467–489, doi:10.1256/smsqj.53810.

We thank the Referee for his/her time and his/her constructive comments. We have complied with most of the proposed changes. In the following, the comments made by the referees appear in black, while our replies are in blue.

General comments

This is a very interesting contribution that builds upon very recent work (e.g. Oertel et al. 2020, Harvey et al. 2020) on the structure and dynamical importance of embedded convection within the warm conveyor belts in extratropical cyclones. In this contribution the authors make use of convection permitting numerical models and field campaign observations to investigate the convective activity in the Stalactite cyclone observed in 2016. This is without doubt relevant research within the scope of WCD. The paper is very well structured and written, and, in my opinion, the description of the methodology is sufficiently complete to allow their reproduction by fellow scientists. Therefore I recommend the article for publication in Weather and Climate Dynamics after revision. I include a list of comments that could be considered by the authors to hopefully enhance the paper. The most important of these is related to the analysis of on-line trajectories. It would be very valuable if the authors can go deeper into this analysis, and in particular of the mid-level convective anticyclonic trajectories and the strong production of negative potential vorticity.

Specific comments

L366-370 and L462-463: I think aspects of the ascent of the anticyclonic trajectories deserve a lot more explanation. The increase and then decrease of PV in WCBs is associated with the transit of the WCB parcels towards a heating maximum (therefore increasing PV) and the away from it (therefore decreasing PV). To my understanding, this is the case by Methven (2015) in his arguments about the matching PV values between WCB inflow and outflow. The trajectory behaviour shown here is the opposite. By what dynamical means is PV decreasing and then increasing. To me it would suggest the presence of strong cooling. However, the trajectories are strongly ascending by about 4km. It would be very interesting to see the evolution of potential temperature along these trajectories. Further details on the evolution of your trajectories would be a great opportunity to confirm the findings in Harvey et al. (2020). We have checked that the evolution of potential temperature essentially follows the evolution of altitude, i.e., an increase during ascent, which excludes a contribution of strong cooling. We specified that the negative peak in PV encountered by mid-level convection trajectories "differs from the evolution at low levels, which matches the typical increase below the heating maximum and decrease above (Wernli et al. 1997). Instead, the evolution at mid levels is similar to that found by Oertel et al. (2020) for trajectories passing through a region under convective influence." Although the topic appears promising, Referee 1 asks for streamlining the PV discussion thus we prefer not to further develop the analysis here and will focus on the link between midlevel convection and negative PV in another study. Please note that our ascents do not perform a full tropospheric rise, and may therefore differ from the theoretical framework presented by Methven (2015), whose reference has been removed accordingly.

L102 and L108: Please include more details on the initial position of the passive tracers to clarify statements such as '...at each grid cell...' or 'they do not necessarily start in the BL'. Thinking about mismatch between modelled prognostic variables (e.g. Whitehead et al. 2015 doi:10.1002/qj.2389, Saffin et al. 2016 doi:10.1002/qj.2729), is there any indication on how accurate these trajectories are? The sentence Line 102 has been rephrased to "Lagrangian trajectories are computed from three online passive tracers defined at each grid cell of the simulation domain (Gheusi and Stein, 2002). The tracers are initialized with their initial 3-D coordinates and are transported by PPM, a scheme with excellent mass-conservation properties and low numerical diffusion."

L110: While I realise that the clustering method is described in Dauhut et al. (2016) it would be useful to have a few more details in this work. E.g. what connectivity rules are being used in this work? The grid spacing in this work is very different from that. Would it be appropriate to use the same rules? We added "Two grid points sharing a common face, either horizontally or vertically, were considered connected, while diagonal connections were considered only vertically. No size criteria were applied". The clustering tool is the same as that applied by Dauhut et al (2016) to identify updrafts, with the exception of the much higher threshold of 10 m s-1, since the focus of this study was on updrafts reaching the stratosphere.

L125-126: ‘The WCB ascent region. . .” Is this not just the cyclone’s warm sector? Or is there any reason to think that this is just the portion in the warm sector affected by WCB ascent? The warm sector spreads over a much larger area. The area we focused on is really the portion in the warm sector affected by WCB ascent. This result is demonstrated with our trajectory analysis.

L145 and L157 and L445: It is stated that e.g. “[The trajectories] number more than 500000”. I’m not clear on how meaningful the number is. As a reference, can you give the initial number of trajectories? While the number is impressive it would be good to have a sense of what it means in physical (mass, volume) terms. We added ”(out of nearly 3 million tropospheric trajectories contained in the red box, which means that about one sixth are ascending)”.

L161-162: “... corresponding to continuous slantwise ascents in WCBs (i.e., 600 hPa in 48 h...” This is slightly misleading as this is a criteria imposed on the trajectories. It doesn’t mean that continuous slantwise ascent has to occur or is even defined in this way. Furthermore in L175 slantwise ascent does not exceed 250 hPa ascent in 12 h. Perhaps you meant 150 hPa? To be more accurate, we changed to ”... corresponds to the typical slantwise ascent rate used for the identification of WCBs (i.e., 600 hPa in 48 h...”.

L166-168: “Using a high ascent rate of 400 hPa in 2.5 h considered as convective, Rasp et al. (2016) found 55.5% of trajectories meeting the threshold for an autumn storm over the Mediterranean Sea but none for a winter case over the North Atlantic”. It’s not clear what should be concluded from this. The proportions are different between cases and one didn’t show strongly ascending trajectories. How is this to be interpreted? We added ”This shows that the proportion of fast ascents and their intensity varies a lot from case to case”.

L170-171: “This choice is motivated by the objective of determining the nature and characteristics of fast ascents”. Please clarify in what way are the motivation and the chosen threshold linked. The threshold seems justifiable, but arbitrary to me. What would’ve changed if the definition was different? We added ”The specific value of the threshold has been set at a value equal to that used by Oertel et al. (2019) for comparison purposes. The use of another threshold would lead to a change in the proportion between slow and fast ascents.”

L295-297: “This discrepancy shows that the identification of fast ascents based on a pressure criterion focuses on lower levels, so that high vertical velocities at higher levels may not be identified as fast ascents”. I’m not clear on the point that is being attempted here. Does this mean that the clustering analysis is to be preferred to trajectory analysis? There is no preference to be expected here because the approaches are radically different (Eulerian for clustering analysis and Lagrangian for trajectory analysis). The point we wanted to make is the difference in terms of vertical velocity intensity when expressed in m s^{-1} or hPa $(2h)^{-1}$. According to the hydrostatic equation, a vertical velocity of 100 hPa $(2h^{-1})$ (the criterion for fast ascents) is equal to 0.12 m s^{-1} at the surface (using a air density of 1.2 kg m^{-2}) and 0.3 m s^{-1} at 300 hPa (using an air density of 0.45 kg m^{-2}). In the latter case, updrafts with such high values are rare (see Figs. 8 and 10). We added ”(a value of 100 hPa $(2h)^{-1}$ is equal to 0.12 m s^{-1} at the surface and 0.3 m s^{-1} at 300 hPa)”.

L337-339: Related to the previous comment: I think I’m confused here and I’m sure it’s just a matter of rewriting: “Once again, these high-level isolated convective structures are not co-located with rapid segments (black dots) and thus not further discussed here”. This seems to contradict the point near L295 about preferring clustering analysis! Again, we do not have any preference. See our response to your previous comment.

Technical corrections

L10-12: In the context of the abstract alone, this sentence is a little obscure as it talks about specific thresholds and cyclonic flow at lower levels. Perhaps the authors can expand a bit to explain e.g. the meaning of the threshold and the expected behaviour. Is cyclonic flow what was expected? The sentence was developed for clarity.

L27: ‘WVB’ should read ‘WCB’. Fixed.

L32-33: I wonder whether Joos and Wernli (2012) would be a suitable reference here. Added.

L118-119: The exact value here and the colour bar in the figure are enough in this case as the contrast is clear. Thus, I would delete the vague colour description from the text e.g. ‘reddish colours’. Removed.

L119-120: “The WCB outflow region IS EXPECTED to be located. . .” It is not clear whether this is what actually happens. Perhaps ‘expected’ should be deleted? Removed.

L125: For clarity rewrite the sentence. I suggest “.. some discrepancies in the BT values when compared against MSG observations can be found locally.” Changed to ”although with larger extent compared against MSG observations”.

L129-130: It’s not clear how comparable the 6-hourly and 1-hour MSLP locations are. Perhaps you can compare 6-hourly versus 6-hourly to then discuss the hourly data once the comparison has been done. Figure 1 shows 6-hourly MSLP locations with dots for ECMWF and the simulation allowing a direct comparison between the two sets.

L134-135: The Meso-NH simulations are driven by ECMWF analysis so that the simulation predicts well the ECMWF analysis track is not that surprising. We agree. This is no surprise because Meso-NH is a state-of-the art model.

L137: Please clarify how the trajectories are counted. Are they counted throughout the 12-h window, or are they counted at 1600 UTC? Changed to ”The location of air parcels fulfilling the ascent criterion of 150 hPa in 12 h is shown at 16:00 UTC as their spatial frequency”.

L142: Change ‘peaks’ for ‘maxima’. To me ‘peak’ denotes a particularly sharp and spiky maxima. Changed.

L144-145: It is not clear whether the mask is actually the red box in Fig. 2. The sentence has been rephrased to ”The red box in Fig. 2 is used as a mask to select the ascents in the WCB region at 16:00 UTC”

L165-166: “... in another NAWDEX cyclone”. You can be specific on the cyclone in the Oertel et al. (2019) study. In fact, you are specific in the conclusions (L453), but just not here. Changed to ”in the NAWDEX Cyclone Vladiana”.

L170: I suggest changing to the following so that the elements in the sentence are consistent: “The ascent of trajectories that do not meet this criterion is defined as slow.”. Changed according to your suggestion.

L193: What criteria was used to decide on whether a trajectory was cyclonic or anticyclonic? The definition was given by a sentence L196, which was moved to L194.

L203: Add ‘trajectories’ after ‘slow ascent’ or change to ‘slowly ascending trajectories’. Changed to ”few slow ascent trajectories”.

L204-205 and L444: This case has many contrasting features to that described in Martinez-Alvarado et al. (2014). In that work it was the anticyclonic branch that exhibited faster ascent than the cyclonic branch. Accordingly, trajectories ascending faster reached higher isentropic levels. It would be good to know the implications or sources of these contrasting features. Is it just case to case variability or do you think it’s deeper than that? We agree. The differences between the case of Martinez-Alvarado et al. (2014) and our study are numerous. We believe that it is a case by case. The study of a larger number of cases is necessary to be able to estimate the general character of these results.

L268: Delete “given by the iso-0 C”. Removed.

L314-319: What about the melting level? It doesn’t seem to be as clearly defined in the simulations as in the observations. Is this important or not? Why? We added ”The bright band is less defined than in the observation suggesting too little simulated melting of snow into rain.” This signal is more stratiform than convective. Its importance in relation with the convective updrafts discussed in the paper is therefore small.

L342: Add ‘Each one of. . .’ at the beginning of the paragraph. I hope this is what you meant here. Ignore if not. Ignored.

L415: It should read ‘overflown’. However the sentence sounds a little odd. It might be worth separating into two sentences. Rephrased.

L441: “WCB trajectories” Are these really WCB trajectories or simply ascending trajectories satisfying the selection criterion? Changed to ”ascending trajectories satisfying the selection criterion”.

Figure 1: If possible, choose a different colour for the theta_e contours so that the colour is not part of the colour scale. The color scale includes many colors, except white. This is what motivated our choice to use of white to draw the theta_e contours.

Figure 4: It would be helpful to have an altitude v time plot. In the current panels it’s difficult to get a clear picture on where the rapid ascent occurs or the differences in altitude between the two types of ascent. Figure 4 shows the trajectories, but for a random sample only, while Fig. 6a shows the plot of the altitude as a function of the time you request and this for all trajectories.

Figure 6: A way of presenting this that has proven useful in other studies is aligning the trajectories according to their time of maximum ascent to highlight the PV behaviour for a typical trajectory. Thanks for your suggestion. However, we removed the time evolution of PV.

Figure 7 and other figures showing vertical sections: In general, the features below 2 km are very difficult to distinguish. The double hatching is very difficult to see. It might be worth including separate figures for the lowest levels. Somehow the black dots do not look like dots but like incomplete symbols, so I’m not sure whether the image is displaying properly on my screen or not. We improved the readability of these figures. In particular, double hatching and yellow contours have been removed in the vertical sections.

Figure 7 caption: Change ‘iso-0degC’ for ‘0degC’ or simply ‘melting’. Changed to ”melting”.

Figure 11b: It’s very difficult to distinguish the overlapping shading. It might be worth separating into four or perhaps two panels for clarity. We decided to group the trajectories into only three categories. This improves the readability of overlapping shading.

Figure 13: This figure is very difficult to read. Any attempt to simplify it would be much appreciated. We improved the readability of this figure.

Organization of convective ascents in a warm conveyor belt

Nicolas Blanchard[1], Florian Pantillon[1], Jean-Pierre Chaboureau[1], and Julien Delanoë[2]

[1]Laboratoire d'Aérologie, Université de Toulouse, CNRS, UPS, Toulouse, France
[2]LATMOS/IPSL, UVSQ Université Paris-Saclay, Sorbonne Université, CNRS, Guyancourt, France

Correspondence: Jean-Pierre Chaboureau (jean-pierre.chaboureau@aero.obs-mip.fr)

Abstract.

Warm conveyor belts (WCBs) are warm, moist airstreams of extratropical cyclones leading to widespread clouds and heavy precipitation, where associated diabatic processes can influence midlatitude dynamics. Although WCBs are traditionally seen as continuous slantwise ascents, recent studies have emphasized the presence of embedded convection~~and the production of mesoscale bands of negative potential vorticity (PV)~~, the impact of which on large-scale dynamics is still debated. Here, detailed cloud and wind measurements obtained with airborne Doppler radar provide unique information on the WCB of the Stalactite cyclone on 2 October 2016 during the North Atlantic Waveguide and Downstream Impact Experiment. The measurements are complemented by a convection-permitting simulation, enabling online Lagrangian trajectories and 3-D objects clustering. ~~The simulation reproduces well the mesoscale structure of the cyclone shown by satellite infrared observations, while the location of trajectories~~ Trajectories rising by $150\,\mathrm{hPa}$ during a relatively short $12\,\mathrm{h}$ window ~~matches~~ are identified as ascents and examined in the WCB region~~expected from high clouds~~. One third ~~of those trajectories, categorized as fast ascents, further~~ take an anticyclonic turn at upper levels, while two thirds follow the cyclonic flow at lower levels. Identified trajectories that reach a $100\,\mathrm{hPa}(2\mathrm{h})^{-1}$ threshold ~~during their ascent and follow the cyclonic flow mainly~~ are further categorized as fast ascents. They represent one third of the ascents and are located at lower levels ~~. In agreement with radar observations , convective updrafts are found~~ mainly. Both radar observations and simulation reveal the presence of convective updrafts in the WCB ~~and~~ region, which are characterized by moderate reflectivity values up to 20 ~~and~~ dBZ. Fast ascents and updraft objects with vertical velocities above $0.3\,\mathrm{m\,s^{-1}}$ ~~. Updraft objects and fast ascents~~ consistently show three main types of convection in the WCB region: (i) frontal convection along the surface cold front and the western edge of the low-level jet; (ii) banded convection at about $2\,\mathrm{km}$ altitude along the eastern edge of the low-level jet; (iii) mid-level convection below the upper-level jet. ~~Mesoscale PV dipoles with strong positive and negative values are located in the vicinity of convective ascentsand appear to accelerate both low-level and upper-level jets. Both convective ascents and negative PV organize into structures with coherent shape, location and evolution, thus suggesting a dynamical linkage. The results show~~ Frontal and banded convection result in shallow ascents, while mid-level convection contributes to the anticyclonic WCB outflow. The results emphasize that convection embedded in WCBs occurs in a coherent and organized manner rather than as isolated cells.

1 Introduction

Warm conveyor belts (WCBs) are large-scale, continously poleward rising airstreams with significant cloud formation associated with extratropical cyclones (Harrold, 1973). They typically ascend by at least 600 hPa in 48 h (Wernli and Davies, 1997; Madonna et al., 2014) from the lower ~~layers of the~~ troposphere in front of the cyclone surface cold front and concentrate a wide range of cloud diabatic processes leading to strong surface precipitation (Browning, 1999; Eckhardt et al., 2004; Flaounas et al., 2017).

During ~~WVB~~ WCB ascent, latent heating from cloud diabatic processes modifies the structure of ~~potential vorticity (PV)~~ PV across the troposphere. Specifically, diabatic PV production (destruction) below (above) the heating maximum creates vertical PV dipoles within WCBs (Wernli and Davies, 1997; Joos and Wernli, 2012; Madonna et al., 2014). These diabatically generated PV dipoles can have an impact on flow evolution by strengthening the large-scale cyclonic (anticyclonic) circulation in the lower (upper) ~~layers of the~~ troposphere (Pomroy and Thorpe, 2000; Grams et al., 2011; Chagnon et al., 2013). The modification of PV within WCBs is mainly driven by latent heating resulting from condensation and water vapor deposition processes ~~(Chagnon et al., 2013; Martínez-Alvarado et al., 2014; Joos and Forbes, 2016)~~(Joos and Wernli, 2012; Chagnon et al., 2013; Martínez-Alv

According to the classical WCB concept, cloud diabatic processes occur along large-scale slantwise airstreams with ascent rates that do not exceed 50 $\mathrm{hPa\,h^{-1}}$ (e.g., Browning, 1986). However, recent studies highlighted the occurrence of convective motions with faster ascent rates embedded in WCBs (Martínez-Alvarado et al., 2014; Rasp et al., 2016; Oertel et al., 2019). These convective motions are mainly localized along the surface cold front (Martínez-Alvarado et al., 2014; Rasp et al., 2016; Oertel et al., 2019). The associated diabatic heating is more intense than within slantwise WCBs ascents and induces the creation of mesoscale, horizontal PV dipoles with strong positive and negative values (Harvey et al., 2020; Oertel et al., 2020). In a North Atlantic case study, Harvey et al. (2020) suggested that PV dipoles occurring in multiple bands would be the natural result of parallel bands in heating in a larger-scale vertical wind shear environment. In a composite analysis, Oertel et al. (2020) showed that horizontal PV dipoles of a few tens of kilometers in diameter formed at the tropopause level above the center of convective updrafts embedded in a WCB. ~~Although convection is usually associated with isolated clouds, Oertel et al. (2020)~~ They suggested that convectively-produced PV dipoles can merge to form elongated PV structures further downstream and locally accelerate the jet stream at the WCB outflow, thus impacting the upper-level dynamics.

Because of their impact on the large-scale flow, diabatic processes are considered a major source of model uncertainty at midlatitudes. Their representation influences the forecast skill of extratropical cyclones and high-impact weather downstream (Grams et al., 2011; Davies and Didone, 2013; Pantillon et al., 2013; Joos and Forbes, 2016). This motivated the North Atlantic Waveguide and Downstream Impact Experiment (NAWDEX; Schäfler et al., 2018), which took place from 19 September to 16 October 2016 with the use of many international facilities, including the deployment of four instrumented aircraft. The field campaign was specifically designed to investigate diabatic processes within WCBs and the evolution of large-scale flows in order to improve model forecasts over the North Atlantic and downstream over Europe~~in autumn and winter~~.

This study is focused on the WCB of a cyclone known as the Stalactite cyclone (Schäfler et al., 2018) that occurred from 30 September to 3 October 2016 and was well ~~sampled~~ observed during NAWDEX. Maddison et al. (2019) previously showed that the representation of the WCB of the Stalactite cyclone impacts the evolution of the downstream large-scale flow at upper levels. ~~More specifically, the onset of a blocking situation over Scandinavia was found unpredictable in the medium-range forecasts.~~ Here, detailed radar observations of this WCB are combined with a convection-permitting simulation over a large domain to investigate convective ascents and their organization and discuss their relationship with the mesoscale PV dipoles found in their vicinity.

The paper is organized as follows: Section 2 presents the radar observations made during the NAWDEX case study and describes the model simulation and analysis tools. Section 3 then details the identification of the large-scale cloud structure corresponding to the WCB and the Lagrangian trajectories that compose it, with a distinction between slow and fast ascents. Section 4 subsequently focuses on the characterization of the fast ascents that occur in the regions of observation, before generalizing the results to the entire WCB region. Section 5 discusses the impact of coherent convective ascents on the cyclone dynamics. Section 6 concludes the paper.

2 Data and methods

2.1 RASTA observations

RASTA (RAdar Airborne System) is an airborne 95 GHz cloud radar (Delanoë et al., 2013). During the NAWDEX campaign, it was carried aboard the French Falcon 20 aircraft operated by SAFIRE (Service des Avions Français Instrumentés pour la Recherche en Environnement). RASTA measures both reflectivity and Doppler velocity along 3 antennas (nadir, backward and transverse) that allow for measuring three noncollinear Doppler velocities, from which the three wind components are reconstructed. The range resolution is 60 m with a maximum range of 15 km. The integration time is set to 250 ms for each antenna and leads to a temporal resolution of 750 ms between two consecutive nadir measurements. It corresponds to a 300 m horizontal resolution given a typical Falcon 20 speed of $200\,\mathrm{m\,s^{-1}}$. The minimum detectable reflectivity is approximately $-35\,\mathrm{dBZ}$ at 1 km, depending on the antenna, with an accuracy of 1 to 2 dBZ (calibration is done using sea surface echo, Li et al., 2005; Ewald et al., 2019). On the afternoon of 2 October 2016, the aircraft flew over the WCB structure of the Stalactite cyclone ~~(flight 7 of the Falcon 20 aircraft)~~(flight 7 of the Falcon 20 aircraft, Schäfler et al., 2018). Here we use the two legs that crossed the WCB between 14:48 and 15:18 UTC and 15:21 and 16:02 UTC, hereinafter referred to as the 15:00 and 16:00 UTC legs, respectively (see the aircraft track in Fig. 1a).

2.2 Meso-NH convection-permitting simulation

The non-hydrostatic mesoscale atmospheric Meso-NH model (Lac et al., 2018) version 5.3 is run over a domain of 2000 km x 2000 km covering the southeastern part of Greenland, Iceland, the Feroe Islands and the track of the Falcon 20 (Fig. 1). A horizontal grid mesh of 2.5 km is chosen allowing deep convection to be explicitly represented. The vertical grid has 51 levels up to 18 km with a grid spacing of 60 m in the first levels and about 600 m at high altitudes. The simulation uses the fifth order weighted essentially non-oscillatory (WENO) advection scheme (Shu and Osher, 1988) for momentum variables and the piecewise parabolic method (PPM) advection scheme (Colella and Woodward, 1984) for the other variables. Turbulence is parameterized using a 1.5 order closure scheme (Cuxart et al., 2000), shallow convection with an eddy diffusivity mass flux scheme (Pergaud et al., 2009), microphysical processes in cloud with a single-moment bulk scheme (Pinty and Jabouille, 1998) and radiation with the European Centre for Medium-Range Weather Forecasts (ECMWF) code (Gregory et al., 2000). Fluxes exchanged between the surface and the atmosphere are represented by the Surface Externalisée (SURFEX) model (Masson et al., 2013).

The simulation starts at 00:00 UTC, 2 October 2016 when the Stalactite cyclone enters in the southwestern part of the domain and ends at 12:00 UTC, 3 October. Initial and boundary conditions are provided by 6-hourly ECMWF operational analyses with an horizontal resolution close to 9 km over the North Atlantic Ocean. To assess the simulated cloud fields, ~~we use observations from RASTA and the Spinning Enhanced Visible and Infrared Imager (SEVIRI) aboard the geostationary Meteosat Second Generation satellite (MSG). Reflectivities and~~ reflectivities and brightness temperatures (BTs) are calculated from the model hourly outputs and directly compared to the RASTA and ~~MSG~~ Meteosat Second Generation satellite (MSG) observations, respectively. Synthetic reflectivities are computed using a version of the radar simulator developed by Richard et al. (2003) that has been modified to take into account gas absorption occurring at 95 GHz. Synthetic BTs are computed using the radiative transfer model for the TIROS Operational Vertical Sounder (RTTOV) code (Saunders et al., 2018), as done by Chaboureau et al. (2008) among many others. In the following, the results are shown for BT at 10.8 µm, which is mainly sensitive to the ~~temperature of clouds at their top~~ cloud top temperature.

2.3 Online trajectory calculation and clustering tools

Lagrangian trajectories are computed from three online passive tracers ~~initialized~~ defined at each grid cell of the simulation domain (Gheusi and Stein, 2002). The tracers are initialized with their initial 3-D coordinates ~~(Gheusi and Stein, 2002)~~and are transported by PPM, a scheme with excellent mass-conservation properties and low numerical diffusion. Trajectories are analysed during a 12 h window centered ~~on~~ around the time of radar observations at 16:00 UTC. This time window is chosen to ensure that trajectories with high wind speed that cross the observation region at 16:00 UTC remain in the simulation domain. ~~Among them, the WCB trajectories~~Increasing the time window quickly increases the number of incomplete trajectories, which strongly biases their general characteristics. Among the trajectories, ascents are defined as those for which the pressure decreases by at least 150 hPa in 12 h. This ~~criterion~~ threshold is adapted for the 12 h duration of the trajectories from the usual WCB criterion of 600 hPa in 48 h (e.g., Madonna et al., 2014; Martínez-Alvarado et al., 2014; Oertel et al., 2020). In contrast with previous studies, no ~~criterion~~ condition is applied on the initial altitude of ~~WCB trajectoriesthus they~~ trajectories, which thus do not necessarily start in the boundary layer. Furthermore, the 150 hPa threshold does not ensure that selected trajectories perform a full ascent from the lower to the upper troposphere. The selected ascents are thus not all actual WCB trajectories but allow investigating upward motion that would otherwise be excluded with the usual criterion.

The clustering tool developed by Dauhut et al. (2016) is used to identify coherent structures. Here, updraft structures are defined as three-dimensional objects made of connected grid point for which the vertical velocity exceeds an arbitrary threshold. Two grid points sharing a common face, either horizontally or vertically, are considered connected, while diagonal connections are considered only vertically. No size criteria are applied. A threshold set to $0.3\,\mathrm{m\,s^{-1}}$ is found to well identify the base of ~~fast updraft structuresin the WCB.~~ updraft structures. This threshold is about five times higher than the typical ascent velocities of a WCB (around $10\,\mathrm{km}$ in $48\,\mathrm{h}$, i.e., $\approx 0.06\,\mathrm{m\,s^{-1}}$). Similarly, negative PV structures are defined as regions of connected grid points with PV values less than -1 PVU (1 PVU$=10^{-6}\,\mathrm{K\,kg^{-1}\,m^{2}\,s^{-1}}$) and without any size criteria.

3 General characteristics~~of the WCB~~

3.1 Cloud structures and track of the cyclone center

The observed BT in the simulation domain is shown at 16:00 UTC when the Stalactite cyclone was turning northeastward (Fig. 1a). ~~The WCB ascent region is expected to be located in the southeastern quadrant of the domain, where a~~ A wide and elongated band of mainly high clouds ~~are found~~ (BT values less than $-35°$ C~~, in reddish colors in Fig. 1a).~~) indicates the WCB region in the southeastern quadrant of the domain. Mid-level ~~troposphere clouds are also observed in the region~~ clouds with BT values between $-35°$ and $0°$ C ~~(in grey and green). The WCB outflow region is expected to be located further northward in the domain, where two branches can~~ are also observed in the region. High clouds can also be distinguished close to Iceland ~~, one anticyclonic and the other cyclonic. The anticyclonic branch extends towards the northeast of the domain, while the cyclonic branch merges with the cloud head to the westof the domain and wraps~~ further northwestward and suggest the outflow of the anticyclonic WCB branch (Martínez-Alvarado et al., 2014). To the west, high and mid-level clouds wrap cyclonically around the cyclone center and illustrate the cloud head, which possibly merges with the cyclonic WCB branch. Between the WCB ~~ascent~~ region and the cloud head, positive BT values ~~(in blue)~~ locate the dry intrusion ~~where~~ whereas patches of negative BT values show the presence of isolated low-level clouds. The simulation correctly reproduces the main cloud structures (Fig. 1b) although ~~some discrepancies in the BT values can be found locally with MSG observation. The WCB ascent region characterized by~~ with larger extent compared against MSG observations. As expected, the WCB region is characterized by high values of equivalent potential temperature (θ_e) at $1\,\mathrm{km}$ ~~above 300~~ and is well covered by high and mid-level clouds. The ~~separation of the WCB into two branches~~cloudy region further northward, the cloud head and the dry intrusion are also well simulated.

The position of the mean sea level pressure (MSLP) minimum is shown along the $36\,\mathrm{h}$ duration of the simulation (dashed red line in Fig. 1). The MSLP minimum is tracked every $6\,\mathrm{h}$ within a radius of $250\,\mathrm{km}$ from its previous position in the ECMWF analysis and every $1\,\mathrm{h}$ within a radius of $160\,\mathrm{km}$ in the Meso-NH simulation. In the analysis, the Stalactite cyclone heads northward on the morning of 2 October, then jumps northeastward at 18:00 UTC, and finally moves northwestward towards Greenland on 3 October. ~~In the simulation, the track shows much more detail with hourly resolution. In particular, the~~ Thanks to hourly resolution, the simulated track reveals that the jump to the ~~northeastward can be explained by to the presence~~ northeast is explained by the formation of a secondary MSLP minimum, as ~~is the case~~ illustrated at 16:00 UTC ~~(black contours~~ in Fig. 1b~~)~~. Overall, the simulation predicts well the complete track from beginning to end including the jump and the deepening of the cyclone from 968 to about $955\,\mathrm{hPa}$.

3.2 Identification of ~~WCBs~~ascents

The ~~frequency of trajectories fullfilling the WCB~~ location of air parcels fulfilling the ascent criterion of 150 hPa in 12 h is shown at 16:00 UTC as their spatial frequency (Fig. 2). It is integrated on all vertical levels and calculated on coarse meshes of 20 km x 20 km for better visibility. ~~The equivalent potential temperature~~ Surface fronts are identified with θ_e at 1 km altitude ~~is used to locate surface fronts~~ (grey contours). This reveals three high-frequency zones of ~~WCB trajectories~~ascending air parcels.

The first zone is located between 56°–64° N and 28°–15° W above a region of homogeneous and relatively high θ_e. It corresponds to the WCB ~~ascent~~ region overflown by the Falcon 20. Relatively high frequency of ~~trajectories is found into~~ ascents is found in the core of ~~the WCB. Local peaks are~~ this region, with local maxima identified in the middle of the 16:00 UTC leg ~~that crossed the WCB and on the west side of the WCB, near the~~ and along the surface cold front. ~~Few or no WCB trajectories~~ As expected, few or no ascents are detected in the dry intrusion, which is located upstream of the cold front and wraps around the low pressure minimum. ~~A mask is applied on the WCB ascent region to select most of the Lagrangian trajectories identified as WCB in this zone~~ The red box in Fig. 2 is used as a mask to select the ascents in the WCB region at 16:00 UTC~~(red box in Fig. 2). They~~ , which number more than 500 ~~000.~~ 000 (out of nearly 3 million tropospheric trajectories contained in the red box, which means that about one sixth are ascending). Thereafter, only these ~~selected trajectories~~ ascents are discussed.

The second zone is located in the western part of the simulation domain between approximately 54°–64° N and 38°–28° W. It corresponds to the ~~cyclonic branch of the WCB that~~ cloud head, which wraps around the low pressure minimum and ~~forms the cloud head. The cloud head~~ is located above the bent-back front, marked by tight contours of θ_e. The third zone is located further north with two local maxima between 64°–68° N and 40°–25° W. The western maximum follows the Greenland coast, above the surface warm front of the Stalactite cyclone. Some of the ~~WCB trajectories~~ ascents pass over the Greenlandic Plateau (around 66° N between 40°–35° W) ~~. These ascents~~ and are likely due to a combination of warm frontal dynamics and the orographic forcing of Greenland. The eastern maximum is located between Greenland and Iceland around 66° N between 30°–25° W, about 100 km behind the surface warm front. The origin of ~~WCB~~ ascents in the second and the third zones is not addressed here, because the Falcon 20 did not fly over these zones at that time.

3.3 Distinction between slow and fast ascents~~in the WCB~~

The ~~ascent~~ properties of the more than 500 000 selected ~~WCB trajectories~~ ascents are now examined. Following Rasp et al. (2016) and Oertel et al. (2019), trajectories are searched for short periods of enhanced ~~ascent~~upward motion. Figure 3a shows the frequency distribution of the maximum 2 h pressure variation ΔP(2 h) = P(t+1) - P(~~t-2~~t-1) along the trajectories from 11:00–21:00 UTC, a negative value of ΔP(2 h) corresponding to an upward ~~trajectory~~motion. By construction, all trajectories underwent a maximum pressure variation stronger than ~~the~~ 25 hPa in 2 h~~criterion~~. This value corresponds to the typical slantwise ascent rate used for the identification of ~~the WCB trajectories, corresponding to continuous slantwise ascents in~~ WCBs (i.e., 600 hPa in 48 h; Madonna et al., 2014). Two thirds of trajectories underwent ascents between 25 and 100 hPa $2\mathrm{h}^{-1}$, i.e., 1 to 4 times the ~~continuous~~ typical slantwise ascent rate. About 5% of the trajectories reached ascent rates above 200 $\mathrm{hPa}\,2\mathrm{h}^{-1}$ and some even 325 $\mathrm{hPa}\,2\mathrm{h}^{-1}$ (<1%). Such ascent rates have also been identified in recent studies combining convection-permitting simulation and online Lagrangian trajectories. Oertel et al. (2019) showed that 14% and 3% of the WCB trajectories identified in ~~another NAWDEX cyclone~~ the NAWDEX Cyclone Vladiana exceeded the ascent rates of 100 hPa and 320 hPa in 2 h, respectively. Using a high ascent rate of 400 hPa in 2.5 h considered as convective, Rasp et al. (2016) found 55.5% of trajectories meeting the threshold for an autumn storm over the Mediterranean Sea but none for a winter case over the North Atlantic. This shows that the proportion of fast ascents and their intensity varies a lot from case to case.

Hereafter, we define fast ascents as ~~WCB trajectories~~ those reaching at least once ~~ΔP(~~a pressure variation greater than 100 hPa in 2 h ~~) below 100~~ between 10:00 and 22:00 UTC. ~~Trajectories~~ The ascents that do not meet this criterion are defined as slow~~ascents~~. This choice is motivated by the objective of determining the nature and characteristics of fast ascents. The specific value of the threshold has been set at a value equal to that used by Oertel et al. (2019) for comparison purposes. The use of another threshold would lead to a change in the proportion between slow and fast ascents. Thus, among the more than 500 000 trajectories, about one third are categorized as fast ascents. Figure 3b shows that these fast ascents (in orange) had the strongest rise during the 12 h window, with about one hundred approaching 600 hPa in 12 h. However, most of them reached less than 300 hPa in 12 h. This suggests that ~~high ascent rates occur~~ strong upward motion occurs during a short period of time mainly, a typical feature of ~~convective motion. Trajectories with~~ convection. In particular, fast ascents with a limited total rise likely encounter shallow convection, which will be discussed in the following section. In contrast, slow ascents (in blue) did not exceed a 250 hPa rise in 12 h ~~. They correspond to the slantwise ascent of the WCB~~and thus rather correspond to continuous slantwise motion.

3.4 Location of slow and fast ascents~~in the WCB~~

An overview of the ~~ascents that take place in the WCB between 10:00 and 22:00 UTC~~ slow and fast ascents is given in Fig. 4. For sake of visibility, only a sample of ~~slow and fast ascent~~ randomly selected trajectories is shown. At 10:00 UTC most slow ascents are located in the ~~core of the WCB~~ center of the region between 50°–57° N and 20°–15° W (red stars in Fig. 4a). A few isolated slow ascents are located further west, between 53°–56° N and 23°–20° W. Another group of slow ascents is located further north, between 57°–60° N and 25°–20° W. At 16:00 UTC the slow ascents have moved with the large-scale flow and spread over the troposphere in the area overflown by the Falcon 20. Those located at an altitude z<8000 m (in blue, green and yellow) rise continuously and maintain a cyclonic turn until 22:00 UTC. They ~~are part of the~~ appear to wrap around the cyclone center and may belong to the cyclonic branch of the WCB, ~~which merges with the cloud head and wraps around the cyclone center~~although WCB branches are typically considered at the outflow level (Martínez-Alvarado et al., 2014). The slow ascents located higher in the troposphere (z>8000 m, in orange) take an anticyclonic turn and are located at higher latitudes (above 65° N) at 22:00 UTC~~. They are~~ , thus are likely part of the anticyclonic branch of the WCB. ~~Figure 4a suggests that there are more slow ascents with a cyclonic than with an anticyclonic turn.~~

At first sight, Fig. 4b suggests that the fast ascents are co-located with the slow ascents. However, most fast ascents remain in the lower troposphere (z<4000 m, in navy blue) and keep a cyclonic turn during the 12 h window. Fast ascents in the middle troposphere (4000<z<8000 m, in green and yellow) are advected further westward than those remaining in the lower troposphere. Only a few fast ascents, located in the upper troposphere (z>8000 m in orange), show an anticyclonic turn at 22:00 UTC. This suggests that the most elevated ascents, both slow and fast, are advected toward higher latitudes by the upper-level jet stream.

~~To detail~~ To distinguish the location of air parcels between slow and fast ascents, their spatial frequency is shown at 16:00 UTC for anticyclonic trajectories (Fig. 5a and b, respectively) and cyclonic trajectories (Fig. 5c and d, respectively). ~~While the slow and fast ascents partly overlap, for example along the cold front and in the core of the WCB, their location clearly differs depending on whether they belong to the cyclonic or anticyclonic branch of the WCB.~~ The distinction between ~~the two branches~~ cyclonic and anticyclonic trajectories is defined by ~~the curvature of each WCB trajectory~~ their curvature during the last 2 h segment, i.e., between 20:00 and 22:00 UTC. With this definition, about one third ~~of the WCB trajectories are part of the anticyclonic branch~~(two thirds) of ascents are anticyclonic (cyclonic). While the slow and fast ascents partly overlap, along the cold front for instance, their location clearly differs depending on whether they take a cyclonic or anticyclonic turn.

Slow ascents occur over much of the WCB region at 16:00 UTC (Fig. 5a and c). Most of slow ascents with anticyclonic trajectories are found between 60°–62° N and 28°–20° W at that time (Fig. 5a). They account for two fifths of the slow ascents. Slow ~~ascent~~ ascents with cyclonic trajectories are located further northwest and southeast ~~of the WCB~~ (Fig. 5c). They are mostly located in a region ~~of the WCB~~ with relatively high and homogeneous values of θ_e at 1 km altitude, to the east of the dry intrusion. Hereafter, this region is defined as the core of the WCB. In contrast, few slow ~~ascent~~ ascents are located along the western side of the WCB, near the surface cold front~~. They are all part of the cyclonic branch (Fig. 5a).~~ , and all show cyclonic trajectories. This contrasts with the case study of Martínez-Alvarado et al. (2014), who found that the anticyclonic branch of the WCB originates from the cold front.

Fast ascent are mainly located ~~behind~~ along the surface cold front and more particularly in its southern part (Fig. 5b and d). This is consistent with the results obtained with a convection-permitting simulation by Oertel et al. (2019), who also found that the fastest ascents take place along the cold front and in its southernmost part especially. Here, most of the fast ascents ~~belong to the cyclonic branch~~ take a cyclonic turn (Fig. 5d) whereas anticyclonic trajectories account for one fifth of the fast ascents only (Fig. 5b).

3.5 Temporal evolution of the ~~WCB~~ ascents

The temporal evolution of ~~the altitude , the vertical velocity , the graupel mixing ratio and the potential vorticity~~ altitude and vertical velocity along the slow and fast ascents is shown in Fig. 6 ~~along the slow and fast ascents~~ between 10:00 and 22:00 UTC. These two categories are further subdivided between cyclonic and anticyclonic trajectories as explained in the previous subsection. ~~As in Oertel et al. (2019),~~ To investigate the occurrence of convective ~~ascents is also investigated in the WCB. Hereafter~~motion, rapid segments are defined hereafter as the 2 h ~~part of the WCB trajectories which undergo an ascent larger~~ parts of ascents that rise by more than 100 hPa. They are further distinguished and shown separately depending on whether they belong to cyclonic or anticyclonic ascents. Note that, by definition, rapid segments can belong to fast ascents only.

All four categories of ascents exhibit a continuous rise during the 12 h window, as expected for WCB ~~ascents.~~trajectories (Fig. 6a). On average, anticyclonic trajectories are located at higher altitudes than cyclonic trajectories~~(Fig. 6a). The interquartile ranges show a lot of overlap between the slow and fast anticyclonic ascents , as well as between the slow and fast cyclonic ascents. The slow anticyclonic ascents (in green) are located in the middle levels of the troposphere~~. Anticyclonic ascents rise in the mid troposphere from z$\sim$4 km at 10:00 UTC ~~, around 4 of altitude. They rise continuously~~ to z$\sim$8 km at 22:00 UTC. ~~Fast anticyclonic ascents (in blue) are located~~ Among them, fast ascents start $\sim$1 km ~~below until 16:00 UTC then undergo a rapid ascent of 0.5 between 16:00 and 20:00 UTC before joining the slow anticyclonic ascents at 22:00 UTC. Cyclonic WCB trajectories are located~~ lower on average, although the interquartile range shows a lot of overlap. Cyclonic ascents are concentrated in the lower ~~and middle levels of the troposphere at 10:00 UTC,~~ troposphere between the surface and ~~3~~2 km altitude ~~. Slow cyclonic ascents (in yellow) rise continuously~~ at 10:00 UTC and rise to z$\sim$~~6~~4 km at 22:00 UTC. Fast cyclonic ascents ~~(in orange) start close to the surface and undergo a quick ascent of 0.4~~also start $\sim$1 ~~between 12:00 and 17:00 UTC before joining the slantwise ascent of slow cyclonic trajectories.~~

km lower than slow ascents on average but again with large overlap in the interquartile range. The fact that anticyclonic ~~WCB trajectories are located at higher altitude than cyclonic trajectories~~ ascents are located higher than cyclonic ascents is consistent with the results of Martínez-Alvarado et al. (2014) ~~.~~for WCB branches, although only anticyclonic trajectories reach typical altitudes of the WCB outflow here. The large overlap in altitude between ~~anticyclonic trajectories suggests that fast ascents are~~ fast and slow ascents suggests that convection is partly embedded in the ~~WCB slantwise ascent (see the 25–75th percentiles in green and blue in~~ slantwise flow, at least where their location also overlap (Fig. ~~6a). The same conclusion can be drawn for cyclonic trajectories. Although~~ 5). While the altitude of trajectories clearly increases with time – by construction of the ~~WCB~~ selection criterion – the altitude of rapid segments remains ~~concentrated between 1 and 4~~fairly stable with time, centered around 5 and 2 km ~~during the 12 window (see~~ along anticyclonic and cyclonic trajectories, respectively (black and red boxplots in Fig. 6a)~~, which suggests that they are due to the same processes~~. Furthermore, their occurrence evolves but persists during the whole 12 h window (see width of the boxplots).

The vertical velocity signal is not as clear as the altitude signal (Fig. 6b). ~~Except for the rapid segments, which often reach vertical velocities greater than 0.3 , all~~ All four categories of ~~WCB trajectories~~ ascents rise with vertical velocities ~~less than~~ below $0.1\,\mathrm{m\,s^{-1}}$ on average. ~~The graupel content is relatively low and largely remains below 0.1~~Fast and slow ascents do not clearly contrast, which indicates that differences are diluted in the averaging process. In contrast, rapid segments reach vertical velocities of 0.2 ~~(Fig. 6c). It decreases with time along anticyclonic trajectories as those gain altitude, while it remains more stable along cyclonic trajectories, located lower in the troposphere. The graupel content is higher for the rapid segments (boxplots), for which it increases from 15:00~~$\mathrm{m\,s^{-1}}$ on average and greater along anticyclonic than cyclonic trajectories. As for their altitude, the vertical velocity of rapid segments remains fairly stable with time. This suggests that processes responsible for convective motion do not substantially change during the 12 ~~UTC onward. This increase corresponds to an acceleration in vertical velocity and reflects convective motion in the low and middle levels of the troposphere.~~ h window.

~~Finally, potential vorticity (PV) values along WCB trajectories range from 0.2~~Finally, and in contrast with results from Oertel et al. (2019), who found high graupel contents along convective trajectories, values largely remain below 0.1 ~~to 0.7 on~~

~~average (Fig. 6d). However, the interquartile ranges show that PV values reach more than 1.2 but also less than 0 . PV increases along cyclonic trajectories as they rise in the troposphere. This contrasts with the decrease in PV along anticyclonic trajectories, located at higher altitude. Similarly, fast ascents have lower PV values than slow ascents, which are more elevated. This is in agreement with the description made by Wernli and Davies (1997), who described the typical evolution of PV within the WCB of extratropical cyclones as low PV values (∼0.5) in the lower troposphere, an increase in PV with values close to ∼1 in the middle troposphere and a decrease in PV at the WCB outflow with PV values below 0.5 . Here, higher positive PV values occur for rapid segments but also negative PV values between 16:00 and 19:00 UTC. It is interesting to note that only fast ascents with an anticyclonic trajectory sometimes reach negative PV values. This contrasts with the classical view of Wernli and Davies (1997) and suggests the creation of negative PV by convective ascents embedded in the WCB as emphasized by recent studies (Oertel et al., 2020; Harvey et al., 2020)~~$\mathrm{g\,kg^{-1}}$ here, even in rapid segments (not shown). This is consistent with the relatively low values of vertical velocity.

4 Fast ascents in the region of observations

This section focuses on the WCB ~~ascent regions~~ region probed by the Falcon 20 aircraft along the 15:00 UTC and 16:00 UTC legs. Observations, combined with simulation results, allow a more detailed characterization of the ~~fast ascents embedded in the WCB.~~ embedded fast ascents.

4.1 Mesoscale structures at 15:00 UTC

Infrared BT values obtained at 15:00 UTC from the MSG satellite show that the Falcon 20 flew westward from a band of high clouds into the dry intrusion and a few isolated low-level clouds below (Fig. 7a). These values are consistent with the vertical structure of reflectivity measured by RASTA (Fig. 7b). In the western part of the cross-section, the dry intrusion is evidenced by ~~the absence of reflectivity values in the troposphere~~reflectivities below -20 dBZ. Some isolated shallow clouds are actually located below 2 km altitude, under the dry intrusion. The most intense, with reflectivities greater than 15 dBZ suggesting a convective origin, extends over a 20 km width. Cirrus clouds indicated by reflectivities observed up to the aircraft altitude of 8.5 km are at the same location as BT values below $-35°$ C. Reflectivity values then increase below z∼7 km, except at the edges of the cloud. Local peaks up to 20 dBZ are measured at 2 km altitude. They indicate the melting level of frozen hydrometeors into liquid water. Peaks in reflectivity are of the same order of magnitude as observed previously in a WCB and associated with convection (e.g., Oertel et al., 2019). The horizontal wind speed measured by RASTA (black contours in Fig. 7b) allows to approximately locate the jet stream above z∼5 km and the low-level jet around z∼1 km in the cloud structure.

The dry intrusion and the high cloud band are well reproduced by the simulation despite a more meridional inclination of the cloud band (Fig. 7~~c~~b). The location, vertical extent and shape of the simulated cloud structure approximately correspond to the observations. ~~The simulation allows the identification of the frozen hydrometeors in the cloud (here the snow in yellow contours). The melting level given by the iso-0~~Below the dry intrusion, an intense cell, with reflectivity values over 15 dBZ, extends over a 10 km width around 23° ~~C (blue line)~~ W. Another vertically developed, intense cell is simulated near 20° W. It extends above the melting level, which lies about 2 km altitude. The ~~simulation shows the location of the~~ jet stream core ~~as well as the low-level jet. The former~~ is located above the top of the clouds around z$\sim$9 km between 24°–20° W. The ~~latter~~ low-level jet extends from the surface up to z$\sim$2 km over more than 2° of longitude. These horizontal wind structures correspond to those observed. The black dots show the location at 15:00 UTC of the ~~WCB trajectories~~ selected ascents (fast and slow). Most of them are located in the cloud region, which thus corresponds well to the WCB. Some trajectories are located in isolated shallow clouds ~~within~~ below the dry intrusion.

4.2 Fast ascents at 15:00 UTC

In addition to Lagrangian trajectories, fast ascents are identified as updraft objects using the clustering tool with a threshold set to w=0.3 $\mathrm{m\,s^{-1}}$. The base of the updraft objects, the horizontal wind speed and θ_e at 1 km altitude are shown in Fig. 8a. The wind speed emphasizes the low-level jet, which extends approximately between 57°–61° N following the cyclonic flow in the lower troposphere. Four types of updrafts objects are identified. The first type is banded convection extending approximately between 58° –60° N and 24°–20° W along the eastern edge of the low-level jet core, with a base between 1 and 2 km altitude (in orange). The second type is mid-level convection that occurs above the western edge of the low-level jet (in blue and green). The third type is frontal convection that occurs along the western edge of the low-level jet, in its southern part mainly (in light orange). The fourth type consists of a few isolated shallow ~~convection~~ convective cells located to the west of the surface cold front (also in light orange). The location of rapid segments (black dots) is in agreement with these updraft objects. This shows that the ~~clustering and Lagrangian approaches~~ (Eulerian) clustering and (Lagrangian) trajectory analyses used here consistently identify the fast ascents~~embedded in the WCB~~.

Three of the four types of updrafts are found along the simulated 15:00 UTC leg, where convective motions are highlighted by relatively high vertical velocity values (w>0.3 $\mathrm{m\,s^{-1}}$, Fig. 8b). The westernmost cell around 23° W indicates isolated shallow convection, below z$\sim$2 km and ~~topping~~ with cloud tops in the dry intrusion. Frontal convection is located at the western edge of the ~~WCB~~ low-level jet around 22° W, also below z$\sim$2 km. Banded convection is located between 2 and 3 km altitude in the core of the WCB, near 20° W. All three types are associated with regions of simulated reflectivity values greater than 15 dBZ (Fig. 7d). Banded convection also corresponds to a region with a relatively high graupel content larger than 0.02 $\mathrm{g\,kg^{-1}}$ (in light green in Fig. ~~7~~8b). Other regions in the core of the WCB also have a relatively high graupel content, which is associated with a high reflectivity value and a high rain content below (~~light blue contours~~not shown). However, these regions are not located in convective updrafts (w>0.3 $\mathrm{m\,s^{-1}}$). This suggests that the corresponding convective motions occurred upstream of the cross-section before 15:00 UTC.

As in Fig. 8a, isolated shallow, frontal and banded convective structures correspond to the location of rapid segments in Fig. 8b (black dots). In contrast, this is not the case for high-level convective regions located between 5.5–8.5 km around 21.5° W. This discrepancy shows that the identification of fast ascents based on a pressure criterion focuses on lower levels, so that high vertical velocities at higher levels may not be identified as fast ascents ~~.~~ (a value of 100 $\mathrm{hPa\,2h^{-1}}$ is equal to 0.12 $\mathrm{m\,s^{-1}}$ at the surface and 0.3 $\mathrm{m\,s^{-1}}$ at 300 hPa). Even higher, a 2 PVU-contour (in magenta) locate the dynamical tropopause at $z\sim10\,\mathrm{km}$ east of 23° W in the vertical section. ~~A stratospheric intrusion down to z~6 is highlighted further west. The core of the jet stream is located in between, around the tilted 2 contour, where the horizontal PV gradient is strongest (see Fig. 7d and Fig. 8b). The PV~~ The PV contours also highlight the occurrence of ~~mesoscale PV dipoles within the three identified WCB convective regions, similarly to those found by Oertel et al. (2020).~~ positive and negative PV structures in the lower and mid troposphere.

4.3 Mesoscale structures at 16:00 UTC

During the 16:00 UTC leg, the Falcon 20 aircraft left the dry intrusion and flew over the WCB region further north (Fig. 9a). In particular, it overflew part of the band of high cloud between 60° - 63° N. A vertical section of reflectivity measured by RASTA along this leg provides more details on the internal structure of the WCB clouds (Fig. 9b). Reflectivity values around $z\sim8\,\mathrm{km}$ correspond to the presence of the high clouds observed by MSG. Under these high clouds are low and middle layer clouds highlighted by larger, positive reflectivity values. Peaks up to $20\,\mathrm{dBZ}$ suggest the presence of convection in the middle troposphere. Below, the bright band again emphasizes that the melting level is localized around $z\sim2\,\mathrm{km}$. Some low and middle layer clouds are located further west, at the edge of the WCB and into the dry intrusion. There, convection forms narrow, vertically extended structures of reflectivity values above $10\,\mathrm{dBZ}$. Their width is between 10 and $20\,\mathrm{km}$ and their height is about $2\,\mathrm{km}$. Horizontal wind speed values above $40\,\mathrm{m\,s^{-1}}$ indicate that the jet stream extends between $z\sim5\,\mathrm{km}$ from the dry intrusion to $z\sim8\,\mathrm{km}$ within the WCB. The jet stream core is not visible in radar imagery because it does not contain clouds. In contrast, the low-level jet is clearly seen and characterized by horizontal wind speed values greater than $30\,\mathrm{m\,s^{-1}}$. It extends horizontally for more than $500\,\mathrm{km}$ and vertically between the surface and $z\sim2\,\mathrm{km}$ inside the cloud structure.

As at 15:00 UTC, the dry intrusion and cloud structures observed by MSG at 16:00 UTC are well reproduced by the model (Fig. 9c). Once again, the large majority of ~~WCB trajectories~~ ascents issued from the ~~Lagrangian~~ trajectory analysis corresponds to the cloud areas. The vertical section of radar reflectivity is also fairly well reproduced by the model, although the horizontal extent of the clouds is more limited in the simulation (Fig. 9d). Around 60° N, two narrow, vertically extended cells of reflectivity values above $10\,\mathrm{dBZ}$ mimic the observation with similar width and height. The bright band is less defined than in the observation suggesting too little simulated melting of snow into rain. Compared to 15:00 UTC, both clouds and ~~WCB trajectories~~ ascents reach higher altitudes (up to $z\sim10\,\mathrm{km}$). As for the simulated jet stream, it is less extended above the cloud structure than at 15:00 UTC. Its core is smaller and located at the western edge of the WCB, which is consistent with the higher cloud tops (compare Figs. 7d and 9d). Finally, the intensity and horizontal extent of the simulated low-level jet at 16:00 UTC correspond to those measured by the Falcon 20.

4.4 Fast ascents at 16:00 UTC

The convective objects described at 15:00 UTC are advected northwestard at 16:00 UTC by the large-scale cyclonic flow (Fig. 10a). Banded convection is still located along the eastern edge of the low-level jet. Between 15:00 and 16:00 UTC, more mid-level ~~convection~~ convective cells formed above the northwestern edge of the low-level jet. Frontal convection is still located along the southwestern edge of the low-level jet and the cold front, while isolated shallow convective cells are found further southwestward. A vertical cross section along the 16:00 UTC leg largely misses convective structures in the simulation (not shown). Its position is therefore shifted 0.5° westward to better capture convective structures close to the WCB areas overflown by the Falcon 20.

As for 15:00 UTC, simulated convective structures are highlighted by vertical velocity values greater than $0.3\,\mathrm{m\,s^{-1}}$ at 16:00 UTC (Fig. 10b). ~~Two~~ A mid-level ~~convection cells are~~ convective cell is identified near the western edge of the WCB, around 60° N. ~~The first cell~~ It extends between $3<z<$~~5~~6.5 km and resembles the ~~deep convective cloud overflown~~ convective cloud at the western edge of the WCB~~by the Falcon 20 (Fig. 9b). The second cell is located between $5<z<6.5$ and may correspond to the western edge of the WCB ,~~, where reflectivity values greater than 15 dBZ were measured by RASTA (Fig. 9b). ~~As found previously for low-level convection, a PV dipole is formed around the two mid-level convective cells. The negative and positive poles are located to the west and east of the ascent, respectively. This is also consistent with the findings of~~ Positive and negative PV structures are present around the cell, which reminds of the horizontal PV dipoles centered around composites of convection embedded in WCB found by Oertel et al. (2020). Three other convective cells are identified above 6 km and up to 9 km altitude in the core of the WCB, around 60.5° N in the vertical section. Once again, because of the identification of fast ascents based on a pressure criterion, these high-level isolated convective structures are not co-located with rapid segments (black dots) and thus not further discussed here.

4.5 Generalization to all identified updraft objects

~~Here, the results~~ Results obtained from the study of updraft objects identified in Figs. 8b and 10b are generalized to all updraft objects located in the vicinity of observations at 16:00 UTC. Three main regions of organized convection are selected (Fig. 10a). The first region (in blue) covers much of the eastern edge of the low-level jet, where banded convection occurs. The second region (in dark green) covers the northwestern part of the low-level jet core, where mid-level convection takes place. The third region (in yellow) covers the southwestern part of the low-level jet, where frontal convection is found. Note that the three regions largely encompass the rapid segments occurring in the vicinity of observations at 16:00 UTC. The isolated shallow convective cells identified before are partly included in the ~~front~~ frontal convection region but do not significantly contribute and are too rare to constitute an extra category.

The three selected regions contain about the same number of ~~fast WCB trajectories~~ rapid segments (∼2800). ~~Cyclonic and anticyclonic sub-categories are further defined for the mid-level convection.~~ Time evolutions of altitude and ~~potential vorticity~~ PV are shown in Fig. 11 along the ~~Lagrangian~~ corresponding trajectories associated with each region. The altitude (Fig. 11a) confirms ~~that frontal and banded convection categories are located in the lower troposphere~~ the location of the three convection categories at 16:00 UTC~~whereas mid-level convection subcategories are located in the middle troposphere~~. All categories show consistent evolution with small interquartile range and are thus relevant. Banded convection (in blue) and frontal convection (in yellow) originate in the lower troposphere at 10:00 UTC. The banded convective trajectories slowly ascend the lower layers of the troposphere and are located at z∼1.5 km on average at 15:00 UTC while the frontal convective trajectories have not started their ascent yet. Both categories finally undergo a rapid rise between 15:00 and 17:00 UTC and reach higher altitudes (z∼3 km and z∼2 km on average for the banded convective cells and the frontal convective cells, respectively) before stabilizing in the lower troposphere until 22:00 UTC. The mid-level convective trajectories are already located at $3<z<4$ km on average at 10:00 UTC ~~. They rise to more than 6~~and rise to 7–8 km ~~and 8~~ of altitude on average at 22:00 UTC~~for the cyclonic and anticyclonic subcategories, respectively~~. These results suggest that trajectories associated with banded and frontal convection at lower levels encounter shallow convection rather than actual WCB ascent. In contrast, trajectories associated with mid-level convection reach typical heights of WCB outflow and thus likely belong to full tropospheric ascents.

Time evolutions of PV for the banded and frontal convection show positive peaks between 1 and 1.5 PVU on average at 16:00 UTC during the ~~rapid~~ quick rise (in blue and yellow in Fig. 11b). The third quartile indicates PV values greater than 4 PVU in the frontal convective regions. This demonstrates that PV is created in these two convective regions. ~~Low graupel content (less than 0.02 on average) is produced above the melting level during the rapid rise (not shown). A similar evolution is found for~~ In contrast, the time evolution of PV for the mid-level ~~cyclonic convection (in green) but with a lower PV production at~~ convection shows a decrease until 16:00 UTC~~(about 0.6 on average). Although located about 1 higher only, mid-level anticyclonic convection (in orange) reaches negative PV values between 15:00 and 17:00 UTC. The~~ , when its average reaches zero and the first quartile even ~~indicates a negative PV~~ shows a negative peak below -1 PVU ~~at 16:00 UTC. It is interesting to note that the PV values are approximately the same at the beginning and end of the WCB trajectories for all categories despite the contrasting evolution . This is consistent with the theoretical study of Methven (2015), who argues that the average PV values should be equal in WCB inflow and outflow regions.~~ (in green). This differs from the evolution at low levels, which matches the typical increase below the heating maximum and decrease above (Wernli and Davies, 1997). Instead, the evolution at mid levels is similar to that found by Oertel et al. (2020) for trajectories passing through a region under convective influence.

Finally, the path followed by trajectories associated with the three selected regions is shown between 10:00 and 22:00 UTC (Fig. 12). For sake of visibility, only a small sample of trajectories is plotted. Banded convection shows trajectories that remain coherent over time ~~in the WCB core. Frontal convection turns northward to follow the banded convective trajectories~~ and is followed by frontal convection trajectories that turn northward around 14:00 UTC~~, while mid-level convection remains localized at the western edge of the WCB~~ . Mid-level convection trajectories remain localized further westward with increasing separation from the other categories during the 12 h window. ~~Most convective trajectories follow the cyclonic branch~~ Banded and frontal convection trajectories follow a cyclonic path and are therefore part of the 26% of cyclonic fast ascents~~that constitute the WCB~~. In contrast, the ~~anticyclonic~~ mid-level ~~convective category is thus part of~~ convection category is split between a majority of anticylonic trajectories, which thus belong to the 8% of anticyclonic fast ascents~~that constitute the WCB~~, and a minority of cylonic trajectories. The bifurcation between ~~mid-level convective trajectories that take an anticylonic and cyclonic curvature at~~ these trajectories depends on altitude, the lower ones keeping a cyclonic curvature until the end of the time window~~depends on altitude~~. The fact that ~~the two~~ both anticylonic and cyclonic mid-level ~~convective subcategories are both~~ convection trajectories are located along the western edge of the WCB at 16:00 UTC is consistent with the overlap of the fast anticyclonic and cyclonic ~~WCB ascents shown in~~ ascents at that time (see green box in in Fig. 5b and d~~, around 28–23 W and 59–61 N. Likewise~~). Similarly, the location of banded and frontal convection in the WCB core at 16:00 UTC is consistent with ~~fast cyclonic WCB ascents in Fig. 5d.~~ the location of fast cyclonic ascents at that time (blue and yellow boxes).

5 ~~Discussion~~Presence of negative PV structures

This ~~discussion focuses on~~ section discusses the possible impact of ~~fast~~ convective ascents on mesoscale dynamics, inspired by recent studies that have highlighted the presence of mesoscale upper-level negative PV structures close to the jet stream core (Oertel et al., 2020; Harvey et al., 2020). The clustering approach previously used to identify updraft objects is applied here to follow the evolution of mid-level and upper-level negative PV structures, which potentially influence the jet stream and large-scale dynamics. Hereafter, negative PV structures are defined as regions with PV values less than $-1\,\mathrm{PVU}$ in order to obtain coherent PV regions that are straightforward to interpret.

~~The altitude of the top of~~ The top altitude of such structures is shown in zooms following their advection to the northwest at 11:00, 16:00 and 21:00 UTC (Fig. 13a, c and e, respectively). The upper-level wind is overlaid and thus allows a comparison between the location of the negative PV structures and the jet stream. To complete the analysis, the rapid segments occurring at the indicated times are represented by black dots. This makes it possible to discuss the occurrence of the fast ascents embedded in the WCB between 11:00 and 21:00 UTC, thus assessing whether the convective structures characterized at 15:00 and 16:00 UTC are representative of the period studied. Modifications of the PV field in the convective regions ~~and associated impacts on large-scale dynamics~~ are further investigated in vertical sections (Fig. 13b, d and f) selected to cross both rapid segment regions (black dots) and negative PV structures (blue shading) at 11:00, 16:00 and 21:00 UTC (see their locations in Fig. 13a, c and e).

~~The location of the~~ At 11:00 UTC, the location of rapid segments is consistent with that of coherent upper-level negative PV structures (above z=5 km)~~and with that of the head~~, which extend meridionally and follow the eastern side of the jet stream ~~at 11:00 UTC~~ core (Fig. 13a). ~~The upper-level negative PV structures meridionally extend from 54–58 N and 22–19 W at 11:00 UTC and follow the eastern side of the jet stream core, located between 55–57 N and 22–20 W approximately.~~ Frontal and banded convection, previously identified at 16:00 UTC (see Sect. 4.5), are already present at ~~11:00 UTC~~ that time (Fig. 13b). As in Fig. 8, frontal convection is located to the west of the low-level jet core (at 22° W, below 2 km altitude in Fig. 13b), while banded convection is located above the low-level jet core (at z∼2 km around 21.2° W). Mid-level convection is also identified in the WCB between ~~5~~4<z<6 km around 20.2° W. These convective regions are associated with regions of vertical velocity w>0.3 $\mathrm{m\,s^{-1}}$ (~~blue~~ green contours) and PV values larger than 3 PVU. This suggests that PV is produced by convection in these regions. In addition, ~~horizontal PV dipoles (with absolute negative poles)~~ negative PV structures are widespread in the WCB. They remain generally shallow (vertical extent <1 km), especially in lower layers at z∼2 km, while ~~vertically more extended negative PV structures are located~~ they extend further vertically in the upper troposphere. In particular, a "negative PV tower" is located at the western cloudy edge of the WCB and just below the core of the jet stream (around 21.5° W between 4<z<8 km in Fig. 13b). ~~The absence of rapid segments in the negative PV tower at 11~~

At 16:00 UTC~~suggests that it formed earlier and upstream. Nevertheless, these results confirms the findings of Sect. 4.5, i.e., the occurrence of high positive PV values in the lower layers and negative PV values in the upper levels of the troposphere. Furthermore, the coincidence of strong positive or negative PV values with strong winds suggest an impact on mesoscale dynamics by locally accelerating both the~~, the upper-level ~~jet stream and the low-level jet.~~

~~The upper-level~~ negative PV structures extend and rise in altitude ~~at 16:00 UTC~~ following the head of the jet stream, where the maximum horizontal wind speeds are located (Fig. 13c). Negative PV structures take the form of elongated bands and are curved anticyclonically. They continue to extend away from each other in the head of the jet stream~~and are partly overflow~~. They are partly overflown by the Falcon 20 at 16:00 UTC (compare with Fig. 10a). A negative PV tower is still located at the western edge of the WCB~~at 16:00 UTC~~, between $3<z<8\,\mathrm{km}$ around 23.5° W (Fig. 13d). At that time, it clearly corresponds to a mid-level convective region that is characterized by both updrafts ($w>0.3\,\mathrm{m\,s^{-1}}$) ~~where rapid segments occur~~ and rapid segments (black dots). Banded convection is captured further east above the low-level jet and is less ~~extensive~~ extended vertically than at 11:00 UTC. Frontal convection does not appear in the vertical section because it is located further south (see Fig. 13c). ~~The~~

At 21:00 UTC, the elongated negative PV bands eventually thin out and disperse ~~at 21:00 UTC~~ while the head of the jet stream disappears (Fig. 13e). Only mid-level convection still occurs on the western edge of the head of the jet stream at 21:00 UTC. Mid-level convective cells detach from the low-level jet and the core of the jet stream between 16:00 and 21:00 UTC and extend further vertically (Fig. 13f). Those located in the core of the WCB are associated with ~~rapid segments regions~~ regions of rapid segments with high positive PV values, between $3<z<6\,\mathrm{km}$ and 62.8°–61.2° N, while a negative PV tower is again present at the western edge of the WCB, between $2<z<6.5\,\mathrm{km}$ and 60.8°–61.2° N (Fig. 13f).

Altogether, the clustering approach shows that elongated negative PV bands persist for ~~about 10 and suggests that they locally intensify the jet stream. The results also suggest a link between convection and negative PV production, which occurs mainly at the beginning and end of the time window and appears to be related to~~ several hours and are mainly found near the head of the jet stream, which is the region where mid-level convection ~~. Although a cause and effect relationship cannot be proven, the common shape, location and timing of the identified structures and fast ascents suggest that the organization of negative PV depends on the organization of convection.~~ also takes place.

6 Conclusions

This study focuses on the occurrence of convective ascents within the WCB of the Stalactite cyclone that approached Iceland on 2 October ~~2016 and investigates a possible impact on the associated mesoscale and large-scale dynamics.~~ 2016. For this purpose, detailed RASTA radar observations of the WCB cloud structure carried out during the NAWDEX field campaign are combined with a Meso-NH convection-permitting simulation covering the mature phase of the cyclone. The simulated cloud structures are in good spatial and temporal agreement with satellite observations on the large scale and radar observations on the kilometer scale, while the trajectory of the simulated cyclone is also consistent with the ECMWF analysis.

~~Firstly,~~ Online Lagrangian trajectories are followed during a 12 h window centered ~~on~~ around the time of the radar observations~~thanks to an online tool implemented in the Meso-NH model~~. Trajectories rising by 150 hPa in 12 h are defined as ~~WCB trajectories~~ascents, based on the usual WCB pressure criterion of $600\,\mathrm{hPa}\,(48\,\mathrm{h})^{-1}$ (e.g., Madonna et al., 2014) and adapted to the shorter time window and without constraint on the initial or final height. ~~Contrary to what one might expect, WCB trajectories are identified not only in~~ Ascents satisfying the selection criterion are identified in three regions with high clouds:

the WCB region, characterized by high values of θ_e, the ~~WCB ascent regionbut also in the~~ cloud head~~and along the warm front of the cyclone. However, the~~, which wraps around the cyclone center and follows the bent-back front, and a third zone above the surface warm front and with orographic forcing from the Greenland plateau. The focus here is on the WCB ~~ascent~~ region, where aircraft observations took place.

Following Rasp et al. (2016) and Oertel et al. (2019), fast ~~WCB~~ ascents are further distinguished from slow ~~WCB~~ ascents by applying an additional pressure threshold of $100\,\mathrm{hPa}$ in $2\,\mathrm{h}$. This results in one third of fast ascents, with ~~ascents~~ ascent rates between 100–325 hPa in $2\,\mathrm{h}$, among the $\sim$500 000 selected ~~WCB trajectories.~~ trajectories. Fast ascents are concentrated on the western edge of the WCB, close to the surface cold front, while slow ascents are rather distributed on the eastern edge. This is consistent with the results of Oertel et al. (2019) for the NAWDEX case study of Cyclone Vladiana. While two thirds of ~~WCB trajectories~~ ascents – both fast and slow – follow the large-scale cyclonic flow between 10:00 and 22:00 UTC, one third take an anticyclonic curvature when their outflow joins the jet stream at the end of the time window. ~~The temporal evolution of the WCB altitude during the 12 window shows that anticyclonic~~ Anticyclonic ascents are located higher than cyclonic ascents ~~, as in the study of Martínez-Alvarado et al. (2014)~~and reach typical altitudes of the WCB outflow, thus resemble the anticyclonic WCB branch (Martínez-Alvarado et al., 2014). However, contrary to the findings of Martínez-Alvarado et al. (2014), anticyclonic trajectories ~~are located further northward – in~~ originate from the WCB head ~~– than cyclonic trajectories – mainly in the southern part of the WCB. Furthermore, fast ascents are concentrated on the western edge of the WCB, close to the surface cold front, while slow ascents are rather distributed on the eastern edge. This is consistent with the results of Oertel et al. (2019) for the NAWDEX case study of Cyclone Vladiana.~~

~~During their ascent, WCB trajectories~~ rather than from the cold front. Finally, during their rise, the ascents undergo a vertical motion of the order of $0.1\,\mathrm{m\,s^{-1}}$ associated with the production of low graupel contents on average during the $12\,\mathrm{h}$ window. Higher values are reached by rapid segments, ~~defined as the periods during which fast WCB ascents rise above the pressure threshold of 100 (2)$^{-1}$, which~~ which are most often located in the lower troposphere. However, these values ~~remains~~ remain lower than those of convective WCB ascents in Oertel et al. (2019), suggesting case-to-case variability. ~~Finally, potential vorticity increases along cyclonic ascents – located mainly in the lower troposphere – and decreases along anticyclonic ascents – located mainly in the mid and upper troposphere. This evolution corresponds to the classical view of the vertical PV dipole within WCBs described by Wernli and Davies (1997). However, negative values are found along a significant fraction of fast ascents with anticyclonic curvature, suggesting that fast ascents create negative PV within the WCB. This contradicts the classical view but agrees with recent results obtained from convection-permitting simulations (Oertel et al., 2020; Harvey et al., 2020).~~

~~By focusing on fast ascents within the WCB, radar observations allow for better characterization of their dimensions and understanding of their formation. They~~ Radar observations reveal structures of high reflectivity in the lower, middle and upper troposphere, thus provide evidence for the existence of fast ascents. These structures are correctly reproduced by the Meso-NH simulation – as is the bright band near z=2 km – where they are associated with rapid segments and vertical velocity larger than $0.3\,\mathrm{m\,s^{-1}}$. These characteristics suggest that the identified fast ascents are actually convective cells embedded in the WCB.

The observed mesoscale dynamics are also correctly reproduced in the simulation. A clustering analysis based on the identification of coherent 3-D ~~objects having a vertical velocity larger than 0.3~~ updraft objects highlights three main types of organized convection at the time of observations. The first type is located at the southwestern edge of the WCB and coincides with the western edge of the low-level jet. It is named "frontal convection", because of its proximity with the surface cold front, and matches early observations by Browning and Pardoe (1973). The second type is located above and to the east of the core of the low-level jet and is named "banded convection", because it forms a long band that extends over several ~~hundred km~~hundreds of kilometers. The third type is located along the western edge of the WCB below the upper-level jet. It is named "mid-level convection" due to its higher altitude. ~~Isolated low-level convective cells are identified below the dry intrusion but are not analyzed further because they are rare and remote from the core of the WCB. Upper-level convective regions are also identified within the WCB but are not associated with fast WCB trajectories and are therefore not investigated either.~~

~~A Lagrangian analysis can then be used to study the temporal evolution over 12 of the trajectories associated with the three main convective regions.~~ The trajectories participating in frontal and banded convection come from the boundary layer and remain below 3 km altitude~~before undergoing a short but strong PV gain during ascent~~. Their geographical path indicates that they are advected by the cyclonic flow during the whole 12 h study period. In contrast, the trajectories participating in mid-level convection start above ~~2~~3 km and rise ~~to 8.5~~up to 8 km altitude. ~~Those with anticyclonic curvature are located higher and reach negative PV values on average~~ They take an anticyclonic curvature mostly. Frontal and banded convection trajectories thus resemble shallow convective ascents that do not clearly belong to the WCB, while mid-level convection trajectories appear to be part of the WCB outflow. The time evolution of PV shows that frontal and banded convection undergo a short but strong PV gain during ascent, while mid-level convection encounters a decrease in PV at the time of ~~the strong ascent, and should therefore have an impact on the upper-level jet stream~~rapid ascent. Negative values are found along half of the mid-level convection trajectories, suggesting that they are associated with negative PV creation. The former corresponds to the classical view of the vertical PV dipole within WCBs described by Wernli and Davies (1997), while the latter contradicts the classical view but agrees with recent results obtained from mesoscale simulations and observations (Oertel et al., 2020; Harvey et al., 2020).

Identifying the main convective regions near the beginning and end of the 12 h window reveals that the three types of convection found at the time of the observations are representative of the convective motion embedded within the WCB during the whole study period. Furthermore, the clustering analysis highlights the presence of upper-level structures of negative PV in the regions of organized ~~mid-level~~ convection. These ~~upper-level negative PV~~ structures extend horizontally ~~over ∼3and~~ to form elongated bands with anticyclonic curvature, especially at the eastern edge of the jet stream head~~where they accelerate the wind locally. Such negative PV bands~~. They also extend vertically ~~over up to 5 and thus~~ to form "negative PV ~~walls~~towers" in the WCB, ~~especially on its western edge~~ under the jet stream in particular. The elongated negative PV bands persist for ~~about 10~~ several hours before dispersing, as do the convective regions and the jet stream head. ~~Similarly, mesoscale PV dipoles created by frontal and banded convectionin the lower troposphere appear to accelerate the low-level jet locally.~~ The common shape, location and timing between the identified structures and rapid segments suggest that the organization of negative PV bands may be related to the organization of convection. The organized nature of convection in WCBs may thus explain the merging of isolated PV dipoles into coherent structures, whose role in mesoscale dynamics is currently being debated (Oertel et al., 2020; Harvey et al., 2020). However, mid-level convective ascents alternatively coincide with positive and negative PV structures, depending on the considered time. Unlike the composite study of Oertel et al. (2019), the formation of horizontal PV dipoles around convective cells thus does not appear systematic, which calls for a more thorough investigation of negative PV formation within WCBs.

Overall, this study suggests that convection in WCBs mainly consists in coherent and organized convective structures that persist with time rather than isolated convective cells embedded in the large-scale slantwise ascent. Furthermore, mid-level convection is more relevant to full tropospheric WCB ascents than frontal and banded convection, which appear to be restricted to lower-level shallow ascents. The results are obtained through a novel combination of Eulerian clustering and online Lagrangian trajectory analyses applied to a convection-permitting simulation. This combination makes it possible to identify coherent structures~~that would otherwise be missed by Lagrangian trajectory tools alone~~, while elevated convection remains partly absent from the analysis ~~due to the WCB selection method~~ and would require a specific approach. ~~Although strict causality cannot be demonstrated here, a coincidence is found between structures of negative PV and of convection, in agreement with recent studies. The organized nature of convection in WCBs may thus explain the merging of isolated PV dipoles into coherent structures, whose role in mesoscale dynamics is currently being debated (Oertel et al., 2020; Harvey et al., 2020).~~ Further questions remain as to ~~exactly how PV~~ how exactly coherent structures form and dissipate, perhaps due to dynamical instabilities in the jet stream region, and may be addressed with the combined Lagrangian-Eulerian approach presented here.

Data availability. All data are available from the authors upon request.

Author contributions. NB performed the simulation and the analyses, JD provided the observations, and all authors prepared the manuscript.

Competing interests. The authors declare that they have no conflict of interest.

Acknowledgements. Computer resources were allocated by GENCI through Project 90569. The research leading to these results has received funding from the ANR-17-CE01-0010 DIP-NAWDEX project. The SAFIRE Falcon contribution to NAWDEX received direct funding from L'Institut Pierre-Simon Laplace (IPSL), Météo-France, Institut National des Sciences de l'Univers (INSU) via the LEFE program, EUFAR Norwegian Mesoscale Ensemble and Atmospheric River Experiment (NEAREX), and ESA (EPATAN, Contract 4000119015/16/NL/CT/gp). We thank the anonymous reviewers for their comments, which helped to improve the overall quality of the paper.

References

Browning, K. A.: Conceptual Models of Precipitation Systems, Wea. Forecasting, 1, 23–41, https://doi.org/10.1175/1520-0434(1986)001<0023:CMOPS>2.0.CO;2, https://doi.org/10.1175/1520-0434(1986)001<0023:CMOPS>2.0.CO;2, 1986.

Browning, K. A.: Mesoscale Aspects of Extratropical Cyclones: An Observational Perspective, in: The Life Cycles of Extratropical Cyclones, edited by Shapiro M.A., Grønås S., American Meteorological Society, pp. 265–283, https://doi.org/10.1007/978-1-935704-09-6_18, 1999.

Browning, K. A. and Pardoe, C. W.: Structure of low-level jet streams ahead of mid-latitude cold fronts, Quart. J. Roy. Meteor. Soc., 99, 619–638, https://doi.org/10.1002/qj.49709942204, http://doi.wiley.com/10.1002/qj.49709942204, 1973.

Chaboureau, J.-P., Söhne, N., Pinty, J.-P., Meirold-Mautner, I., Defer, E., Prigent, C., Pardo, J.-R., Mech, M., and Crewell, S.: A midlatitude cloud database validated with satellite observations, J. Appl. Meteor. Climatol., 47, 1337–1353, https://doi.org/10.1175/2007JAMC1731.1, https://doi.org/10.1175/2007JAMC1731.1, 2008.

Chagnon, J. M., Gray, S. L., and Methven, J.: Diabatic processes modifying potential vorticity in a North Atlantic cyclone, Quart. J. Roy. Meteor. Soc., 139, 1270–1282, https://doi.org/10.1002/qj.2037, https://rmets.onlinelibrary.wiley.com/doi/abs/10.1002/qj.2037, 2013.

Colella, P. and Woodward, P. R.: The Piecewise Parabolic Method (PPM) for gas-dynamical simulations, J. Comput. Phys., 54, 174–201, https://doi.org/doi.org/10.1016/0021-9991(84)90143-8, http://www.sciencedirect.com/science/article/pii/0021999184901438, 1984.

Cuxart, J., Bougeault, P., and Redelsperger, J.-L.: A turbulence scheme allowing for mesoscale and large-eddy simulations, Quart. J. Roy. Meteor. Soc., 126, 1–30, https://doi.org/10.1002/qj.49712656202, https://doi.org/10.1002/qj.49712656202, 2000.

Dauhut, T., Chaboureau, J.-P., Escobar, J., and Mascart, P.: Giga-LES of Hector the Convector and its two tallest updrafts up to the stratosphere, J. Atmos. Sci., 73, 5041–5060, https://doi.org/10.1175/JAS-D-16-0083.1, https://doi.org/10.1175/JAS-D-16-0083.1, 2016.

Davies, H. C. and Didone, M.: Diagnosis and Dynamics of Forecast Error Growth, Mon. Weather Rev., 141, 2483–2501, https://doi.org/10.1175/MWR-D-12-00242.1, https://doi.org/10.1175/MWR-D-12-00242.1, 2013.

Delanoë, J., Protat, A., Jourdan, O., Pelon, J., Papazzoni, M., Dupuy, R., Gayet, J.-F., and Jouan, C.: Comparison of airborne in situ, airborne radar-lidar, and spaceborne radar-lidar retrievals of polar ice cloud properties sampled during the POLARCAT campaign, J. Atmos. Ocean Technol., 30, 57–73, https://doi.org/10.1175/JTECH-D-11-00200.1, https://doi.org/10.1175/JTECH-D-11-00200.1, 2013.

Eckhardt, S., Stohl, A., Wernli, H., James, P., Forster, C., and Spichtinger, N.: A 15-Year Climatology of Warm Conveyor Belts, J. Climate, 17, 218–237, https://doi.org/10.1175/1520-0442(2004)017<0218:AYCOWC>2.0.CO;2, https://doi.org/10.1175/1520-0442(2004)017<0218:AYCOWC>2.0.CO;2, 2004.

Ewald, F., Groß, S., Hagen, M., Hirsch, L., Delanoë, J., and Bauer-Pfundstein, M.: Calibration of a 35 GHz airborne cloud radar: lessons learned and intercomparisons with 94 GHz cloud radars, Atmos. Meas. Tech., 12, 1815–1839, https://doi.org/10.5194/amt-12-1815-2019, https://doi.org/10.5194/amt-12-1815-2019, 2019.

Flaounas, E., Kotroni, V., Lagouvardos, K., Gray, S., Rysman, J., and Claud, C.: Heavy rainfall in Mediterranean cyclones. Part I: contribution of deep convection and warm conveyor belt, Climate Dynamics, https://doi.org/10.1007/s00382-017-3783-x, 2017.

Gheusi, F. and Stein, J.: Lagrangian description of airflows using Eulerian passive tracers, Quart. J. Roy. Meteor. Soc., 128, 337–360, https://doi.org/10.1256/00359000260498914, http://doi.org/10.1256/00359000260498914, 2002.

Grams, C. M., Wernli, H., Böttcher, M., Čampa, J., Corsmeier, U., Jones, S. C., Keller, J. H., Lenz, C.-J., and Wiegand, L.: The key role of diabatic processes in modifying the upper-tropospheric wave guide: a North Atlantic case-study, Quart. J. Roy. Meteor. Soc., 137, 2174–2193, https://doi.org/10.1002/qj.891, https://rmets.onlinelibrary.wiley.com/doi/abs/10.1002/qj.891, 2011.

Gregory, D., Morcrette, J.-J., Jakob, C., Beljaars, A. M., and Stockdale, T.: Revision of convection, radiation and cloud schemes in the ECMWF model, Quart. J. Roy. Meteor. Soc., 126, 1685–1710, https://doi.org/10.1002/qj.49712656607, http://doi.org/10.1002/qj.49712656607, 2000.

Harrold, T. W.: Mechanisms influencing the distribution of precipitation within baroclinic disturbances, Quart. J. Roy. Meteor. Soc., 99, 232–251, https://doi.org/10.1002/qj.49709942003, https://rmets.onlinelibrary.wiley.com/doi/abs/10.1002/qj.49709942003, 1973.

Harvey, B., Methven, J., Sanchez, C., and Schäfler, A.: Diabatic generation of negative potential vorticity and its impact on the North Atlantic jet stream, Quart. J. Roy. Meteor. Soc., 146, 1477–1497, https://doi.org/10.1002/qj.3747, https://rmets.onlinelibrary.wiley.com/doi/abs/10.1002/qj.3747, 2020.

Joos, H. and Forbes, R. M.: Impact of different IFS microphysics on a warm conveyor belt and the downstream flow evolution, Quart. J. Roy. Meteor. Soc., 142, 2727–2739, https://doi.org/10.1002/qj.2863, https://doi.org/10.1002/qj.2863, 2016.

Joos, H. and Wernli, H.: Influence of microphysical processes on the potential vorticity development in a warm conveyor belt: a case-study with the limited-area model COSMO, Quart. J. Roy. Meteor. Soc., 138, 407–418, https://doi.org/10.1002/qj.934, https://doi.org/10.1002/qj.934, 2012.

Lac, C., Chaboureau, J.-P., Masson, V., Pinty, J.-P., Tulet, P., Escobar, J., Leriche, M., Barthe, C., Aouizerats, B., Augros, C., Aumond, P., Auguste, F., Bechtold, P., Berthet, S., Bieilli, S., Bosseur, F., Caumont, O., Cohard, J.-M., Colin, J., Couvreux, F., Cuxart, J., Delautier, G., Dauhut, T., Ducrocq, V., Filippi, J.-B., Gazen, D., Geoffroy, O., Gheusi, F., Honnert, R., Lafore, J.-P., Lebeaupin Brossier, C., Libois, Q., Lunet, T., Mari, C., Maric, T., Mascart, P., Mogé, M., Molinié, G., Nuissier, O., Pantillon, F., Peyrillé, P., Pergaud, J., Perraud, E., Pianezze, J., Redelsperger, J.-L., Ricard, D., Richard, E., Riette, S., Rodier, Q., Schoetter, R., Seyfried, L., Stein, J., Suhre, K., Thouron, O., Turner, S., Verrelle, A., Vié, B., Visentin, F., Vionnet, V., and Wautelet, P.: Overview of the Meso-NH model version 5.4 and its applications, Geosci. Model Dev., 11, 1929–1969, https://doi.org/10.5194/gmd-11-1929-2018, https://doi.org/10.5194/gmd-11-1929-2018, 2018.

Li, L., Heymsfield, G. M., Tian, L., and Racette, P. E.: Measurements of Ocean Surface Backscattering Using an Airborne 94-GHz Cloud Radar—Implication for Calibration of Airborne and Spaceborne W-Band Radars, J. Atmos. Ocean. Tech, 27, 1033–1045, https://doi.org/10.1175/JTECH1722.1, https://doi.org/10.1175/JTECH1722.1, 2005.

Maddison, J. W., Gray, S. L., Martínez-Alvarado, O., and Williams, K. D.: Upstream Cyclone Influence on the Predictability of Block Onsets over the Euro-Atlantic Region, Monthly Weather Review, 147, 1277–1296, https://doi.org/10.1175/MWR-D-18-0226.1, 2019.

Madonna, E., Wernli, H., Joos, H., and Martius, O.: Warm conveyor belts in the ERA-Interim dataset (1979–2010). Part I: climatology and potential vorticity evolution, J. Climate, 27, 3–26, https://doi.org/10.1175/JCLI-D-12-00720.1, https://doi.org/10.1175/JCLI-D-12-00720.1, 2014.

Martínez-Alvarado, O., Joos, H., Chagnon, J., Boettcher, M., Gray, S. L., Plant, R. S., Methven, J., and Wernli, H.: The dichotomous structure of the warm conveyor belt, Quart. J. Roy. Meteor. Soc., 140, 1809–1824, https://doi.org/10.1002/qj.2276, https://doi.org/10.1002/qj.2276, 2014.

Masson, V., Le Moigne, P., Martin, E., Faroux, S., Alias, A., Alkama, R., Belamari, S., Barbu, A., Boone, A., Bouyssel, F., Brousseau, P., Brun, E., Calvet, J.-C., Carrer, D., Decharme, B., Delire, C., Donier, S., Essaouini, K., Gibelin, A.-L., Giordani, H., Habets, F., Jidane, M., Kerdraon, G., Kourzeneva, E., Lafaysse, M., Lafont, S., Lebeaupin Brossier, C., Lemonsu, A., Mahfouf, J.-F., Marguinaud, P., Mokhtari, M., Morin, S., Pigeon, G., Salgado, R., Seity, Y., Taillefer, F., Tanguy, G., Tulet, P., Vincendon, B., Vionnet, V., and Voldoire, A.: The SURFEXv7.2 land and ocean surface platform for coupled or offline simulation of earth surface variables and fluxes, Geosci. Model Dev., 6, 929–960, https://doi.org/10.5194/gmd-6-929-2013, https://doi.org/10.5194/gmd-6-929-2013, 2013.

Methven, J.: Potential vorticity in warm conveyor belt outflow, Quart. J. Roy. Meteor. Soc., 141, 1065–1071, https://doi.org/10.1002/qj.2393, https://doi.org/10.1002/qj.2393, 2015.

Oertel, A., Boettcher, M., Joos, H., Sprenger, M., Konow, H., Hagen, M., and Wernli, H.: Convective activity in an extratropical cyclone and its warm conveyor belt – a case-study combining observations and a convection-permitting model simulation, Quart. J. Roy. Meteor. Soc., 145, 1406–1426, https://doi.org/10.1002/qj.3500, https://doi.org/10.1002/qj.3500, 2019.

Oertel, A., Boettcher, M., Joos, H., Sprenger, M., and Wernli, H.: Potential vorticity structure of embedded convection in a warm conveyor belt and its relevance for large-scale dynamics, Weather Clim. Dynam., 1, 127–153, https://doi.org/10.5194/wcd-1-127-2020, https://doi.org/10.5194/wcd-1-127-2020, 2020.

Pantillon, F., Chaboureau, J.-P., Lac, C., and Mascart, P.: On the role of a Rossby wave train during the extratropical transition of hurricane Helene (2006), Quart. J. Roy. Meteor. Soc., 139, 370–386, https://doi.org/10.1002/qj.1974, https://doi.org/10.1002/qj.1974, 2013.

Pergaud, J., Masson, V., Malardel, S., and Couvreux, F.: A Parameterization of Dry Thermals and Shallow Cumuli for Mesoscale Numerical Weather Prediction, Bound. Layer. Meteor., 132, 83–106, https://doi.org/10.1007/s10546-009-9388-0, https://doi.org/10.1007/s10546-009-9388-0, 2009.

Pinty, J.-P. and Jabouille, P.: A mixed-phase cloud parameterization for use in a mesoscale non-hydrostatic model: simulations of a squall line and of orographic precipitations, in: Conf. on cloud physics, Everett, WA, Amer. Meteor. Soc., pp. 217–220, 1998.

Pomroy, H. R. and Thorpe, A. J.: The evolution and dynamical role of reduced upper-tropospheric potential vorticity in intensive observing period one of FASTEX, Mon. Weather Rev., 128, 1817–1834, https://doi.org/10.1175/1520-0493(2000)128<1817:TEADRO>2.0.CO;2, https://doi.org/10.1175/1520-0493(2000)128<1817:TEADRO>2.0.CO;2, 2000.

Rasp, S., Selz, T., and Craig, G. C.: Convective and Slantwise Trajectory Ascent in Convection-Permitting Simulations of Midlatitude Cyclones, Mon. Weather Rev., 144, 3961–3976, https://doi.org/10.1175/MWR-D-16-0112.1, https://doi.org/10.1175/MWR-D-16-0112.1, 2016.

Richard, E., Cosma, S., Tabary, P., Pinty, J.-P., and Hagen, M.: High-resolution numerical simulations of the convective system observed in the Lago Maggiore area on 17 September 1999 (MAP IOP 2a), Quart. J. Roy. Meteor. Soc., 129, 543–563, https://doi.org/10.1256/qj.02.50, https://doi.org/10.1256/qj.02.50, 2003.

Saunders, R., Hocking, J., Turner, E., Rayer, P., Rundle, D., Brunel, P., Vidot, J., Roquet, P., Matricardi, M., Geer, A., Bormann, N., and Lupu, C.: An update on the RTTOV fast radiative transfer model (currently at version 12), Geosci. Model Dev., 11, 2717–2737, https://doi.org/10.5194/gmd-11-2717-2018, https://doi.org/10.5194/gmd-11-2717-2018, 2018.

Schäfler, A., Craig, G., Wernli, H., Arbogast, P., Doyle, J. D., McTaggart-Cowan, R., Methven, J., Rivière, G., Ament, F., Boettcher, M., Bramberger, M., Cazenave, Q., Cotton, R., Crewell, S., Delanoë, J., Dörnbrack, A., Ehrlich, A., Ewald, F., Fix, A., Grams, C. M., Gray, S. L., Grob, H., Groß, S., Hagen, M., Harvey, B., Hirsch, L., Jacob, M., Kölling, T., Konow, H., Lemmerz, C., Lux, O., Magnusson, L., Mayer, B., Mech, M., Moore, R., Pelon, J., Quinting, J., Rahm, S., Rapp, M., Rautenhaus, M., Reitebuch, O., Reynolds, C. A., Sodemann, H., Spengler, T., Vaughan, G., Wendisch, M., Wirth, M., Witschas, B., Wolf, K., and Zinner, T.: The North Atlantic Waveguide and Downstream Impact Experiment, Bull. Amer. Meteo. Soc., 99, 1607–1637, https://doi.org/10.1175/BAMS-D-17-0003.1, https://doi.org/10.1175/BAMS-D-17-0003.1, 2018.

Shu, C.-W. and Osher, S.: Efficient implementation of essentially non-oscillatory shock-capturing schemes, J. Comput. Phys., 77, 439–471, https://doi.org/10.1016/0021-9991(88)90177-5, https://doi.org/10.1016/0021-9991(88)90177-5, 1988.

Wernli, H. and Davies, H. C.: A Lagrangian-based analysis of extratropical cyclones. I: The method and some applications, Quart. J. Roy. Meteor. Soc., 123, 467–489, https://doi.org/10.1002/qj.49712353811, https://doi.org/10.1002/qj.49712353811, 1997.

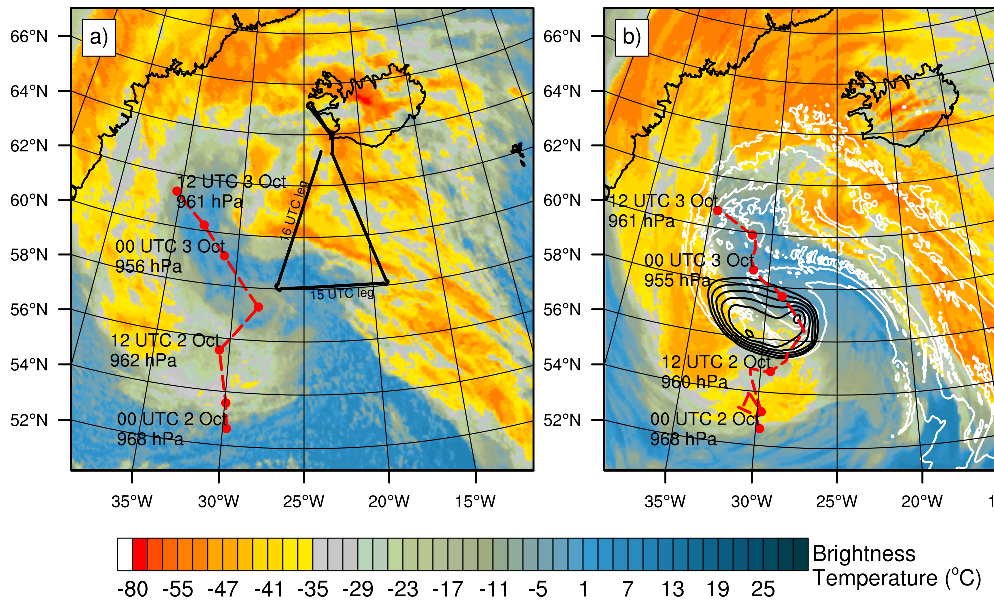

Figure 1. 10.8 μm brightness temperature (in $^{\circ}$C) at 16:00 UTC (a) observed ~~by SEVIRI on the~~ from MSG ~~satellite~~ (raw data courtesy of EUMETSAT) and (b) simulated by Meso-NH. In (a) and (b), ~~the position and value of the MSLP minimum~~ cyclone track is shown (red dotted line, red mark every ~~3~~6 h and MSLP minimum value every 12 h) for the ECMWF analysis and the Meso-NH simulation, respectively. In (a), the black line shows the track of the Falcon 20 aircraft and the 15:00 and 16:00 UTC legs. In (b), MSLP is shown with black contours every 1 hPa between 959 and 964 hPa and θ_e at 1 km altitude with white contours every 4 K between 300 and 316 K.

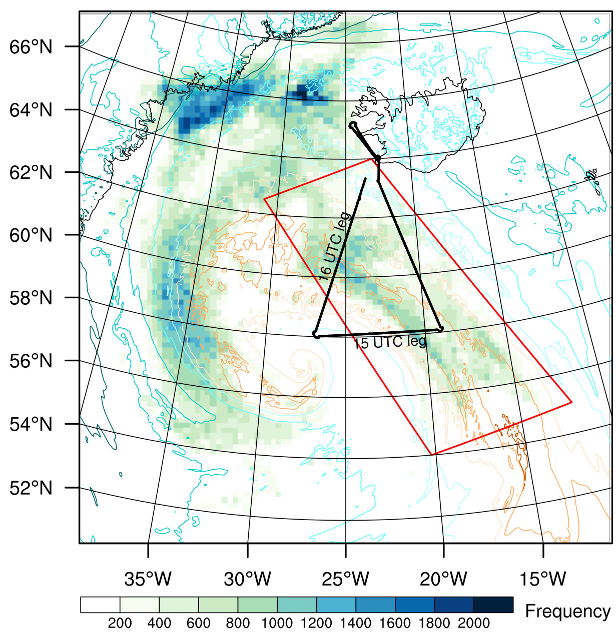

Figure 2. ~~WCB~~ Spatial frequency of air parcels belonging to identified ascents (shading) and θ_e at 1 km altitude (~~grey~~ colored contours every 4 K between 288 and ~~316~~312 K), all at 16:00 UTC. The black lines show the track of the Falcon 20 aircraft and the 15:00 and 16:00 UTC legs. The ~~selected WCB trajectories are contained in the~~ red box illustrates the mask used to focus on the WCB region.

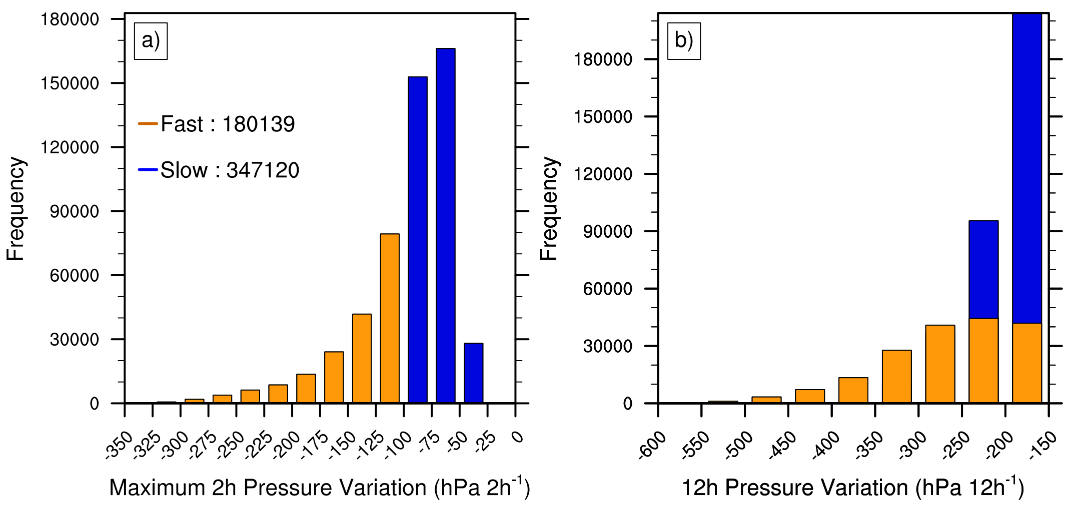

Figure 3. Histograms of (a) maximum 2 h pressure variation ($\mathrm{hPa}\,2\mathrm{h}^{-1}$) and of (b) 12 h pressure variation ($\mathrm{hPa}\,12\mathrm{h}^{-1}$) along the ~~more than 500 000~~ selected ~~WCB trajectories~~ascents. Slow ascents are shown in blue and fast ascents in ~~dark~~ orange.

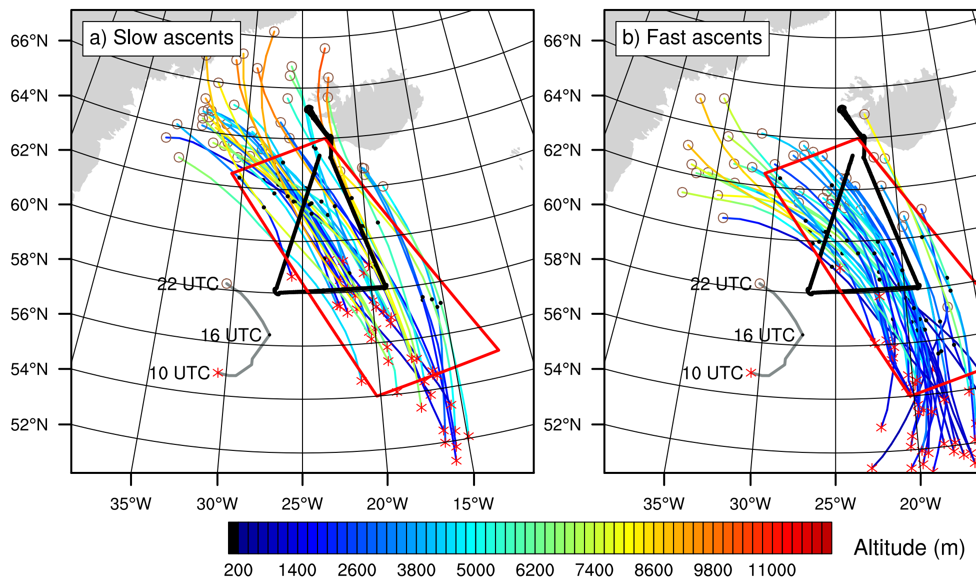

Figure 4. ~~WCB~~ Selected trajectories ~~as a function of~~ colored by altitude between 10:00 and 22:00 UTC for (a) slow ascents and (b) fast ascents. Only 40 trajectories are plotted for each category~~of ascents~~. Red crosses, black dots and brown circles show the location of the trajectories at 10:00, 16:00 and 22:00 UTC, respectively. The black lines show the track of the Falcon 20 aircraft, the grey curve the position of the MSLP minimum and the red box the region where the ~~WCB~~ trajectories are selected at 16:00 UTC.

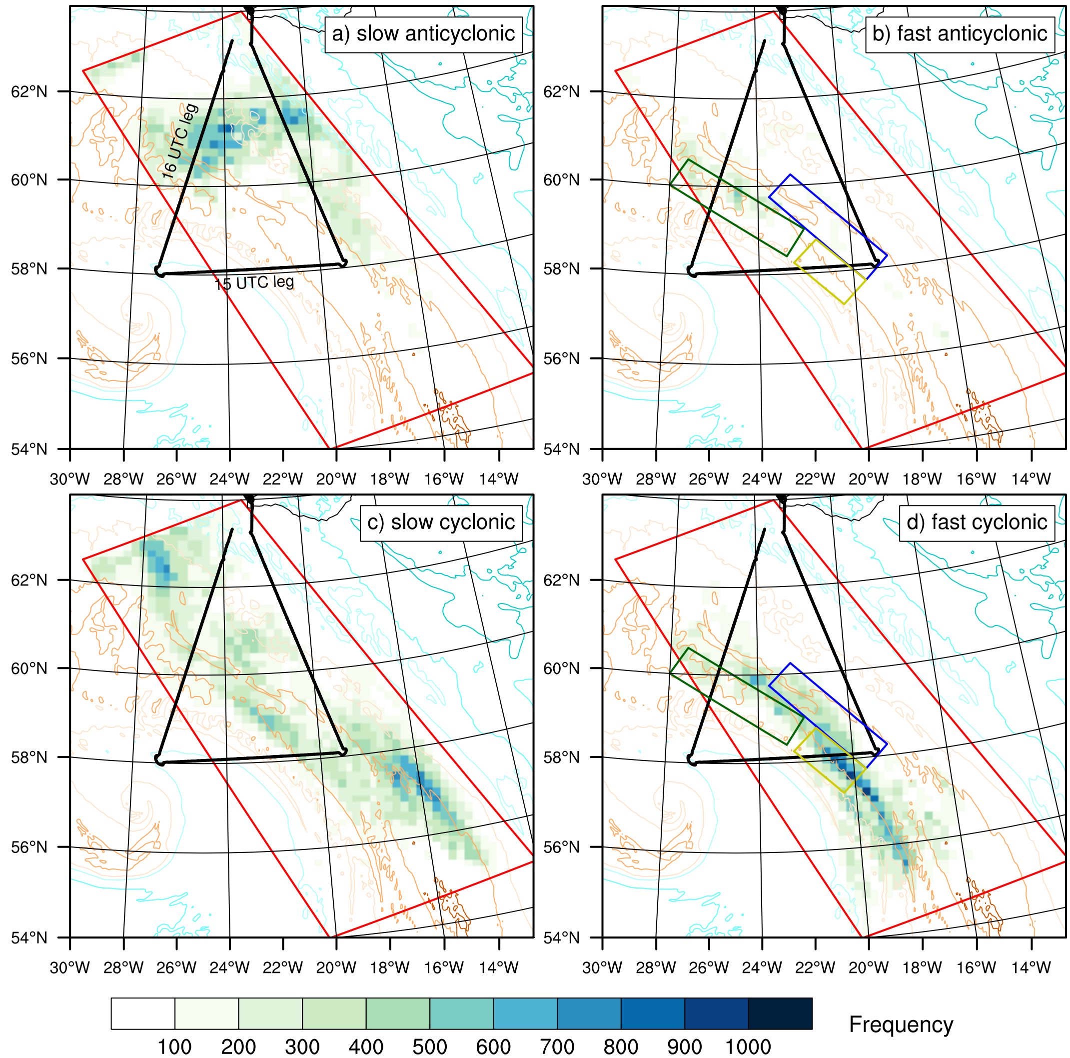

Figure 5. As in Fig. 2 but for slow ascents with (a) anticyclonic and (b) cyclonic curvature and fast ascents with (c) anticyclonic and (d) cyclonic curvature zoomed on the ~~selected WCB~~ region of selection (red box). In (b and d), the dark green, yellow and blue boxes are displayed for comparison with Fig. 10.

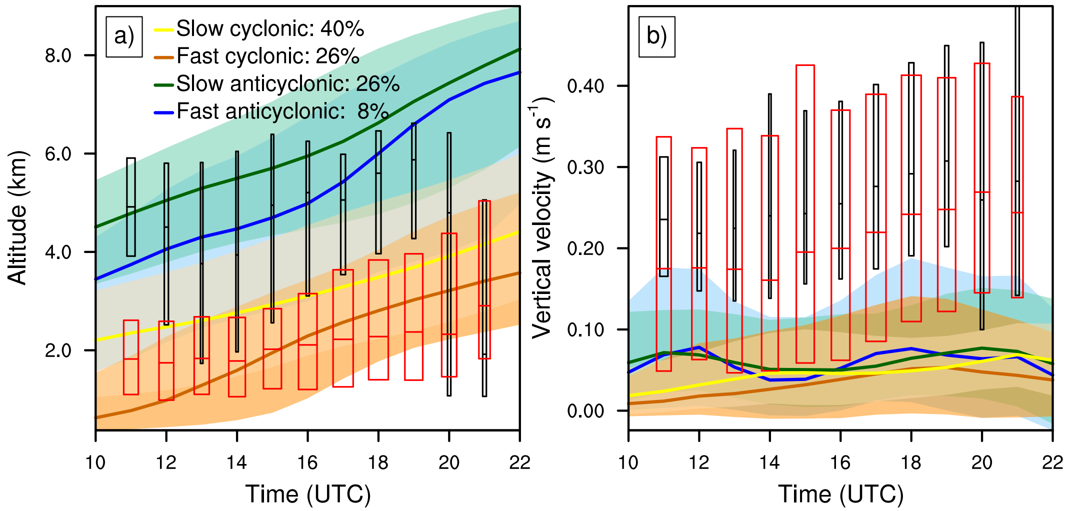

Figure 6. Temporal evolution of (a) altitude (in km) ~~,~~ and (b) vertical velocity (in $\mathrm{m\,s^{-1}}$) ~~, (c) graupel mixing ratio (in) and (d) potential vorticity (in)~~ between 10:00 and 22:00 UTC. The median (colored bold curves) and the 25th–75th percentiles (shaded colors) are shown for slow cyclonic (yellow), fast cyclonic (red), slow anticyclonic (green) and fast anticyclonic (blue) ascents. The median and the 25th–75th percentiles for the 2 h rapid segments are shown with red and black boxplots for cyclonic and anticyclonic trajectories, respectively, with width proportional to their number.

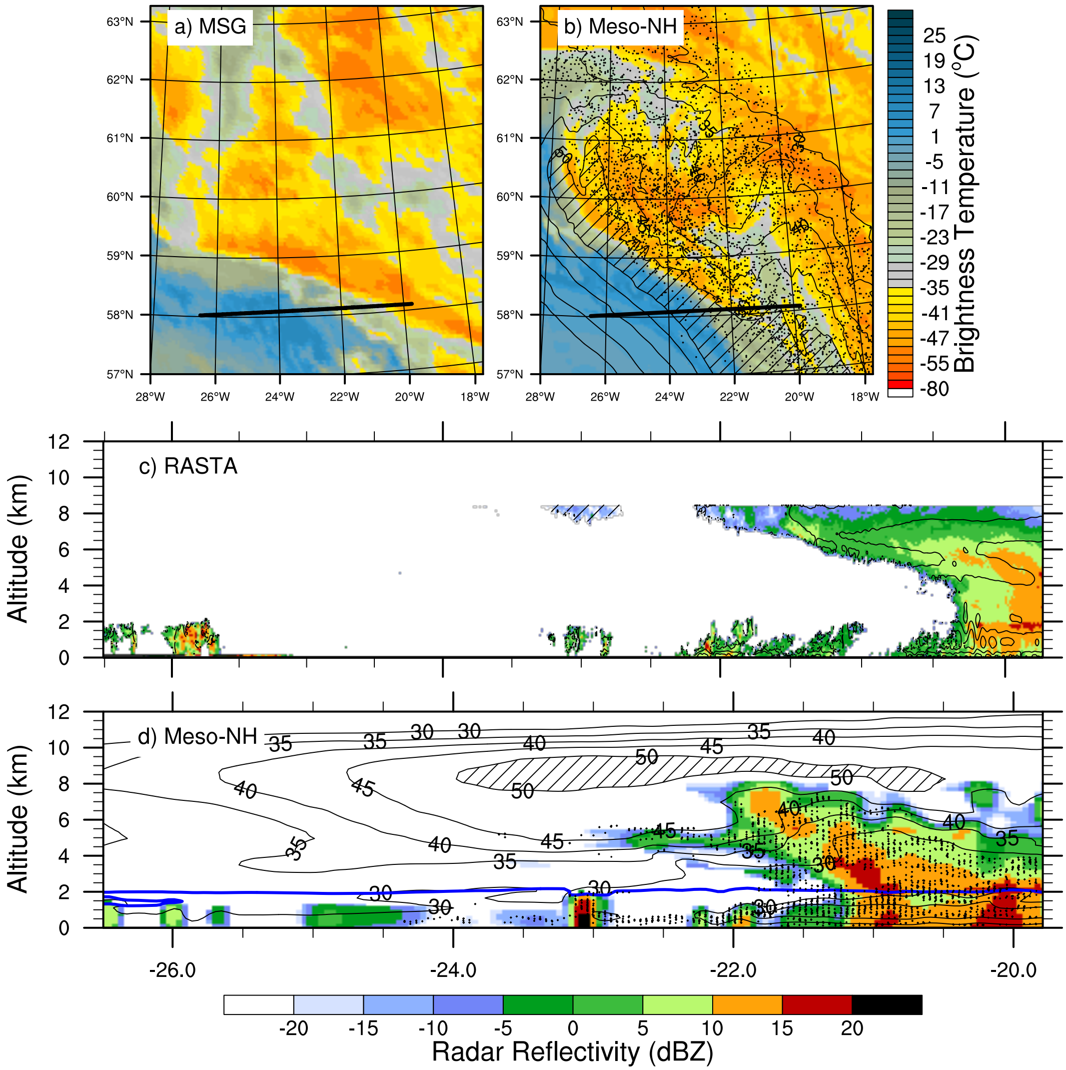

Figure 7. Results at 15:00 UTC. ~~Left column~~Top row: 10.8 μm brightness temperature (in $^\circ$C) (a) observed by MSG (raw data courtesy of EUMETSAT) and (~~c~~b) simulated by Meso-NH. In (~~c~~b), the black contours ~~shows~~ show the horizontal wind speed at 320 K with hatching for values greater than 50 $\mathrm{m\,s^{-1}}$. ~~Right column~~Central and bottom panels: ~~Reflectivity~~ reflectivity (in dBZ) (~~b~~c) measured by RASTA and (d) simulated by Meso-NH along the black line shown in (a) and (~~c~~b), respectively. The black contours show the horizontal wind speed (in $\mathrm{m\,s^{-1}}$) with hatching for values greater than 50 $\mathrm{m\,s^{-1}}$~~and double hatching for values greater than 35 below 2 altitude~~. In (~~c~~b) and (d), the black dots indicate the position of the ~~WCB trajectories~~ ascents (one trajectory every 60 in (~~c~~b)). In (d), the ~~grey and yellow contours show the condensed water and snow contents equal to 0.02 , respectively. The~~ blue contour shows the ~~iso-0 C~~ melting level.

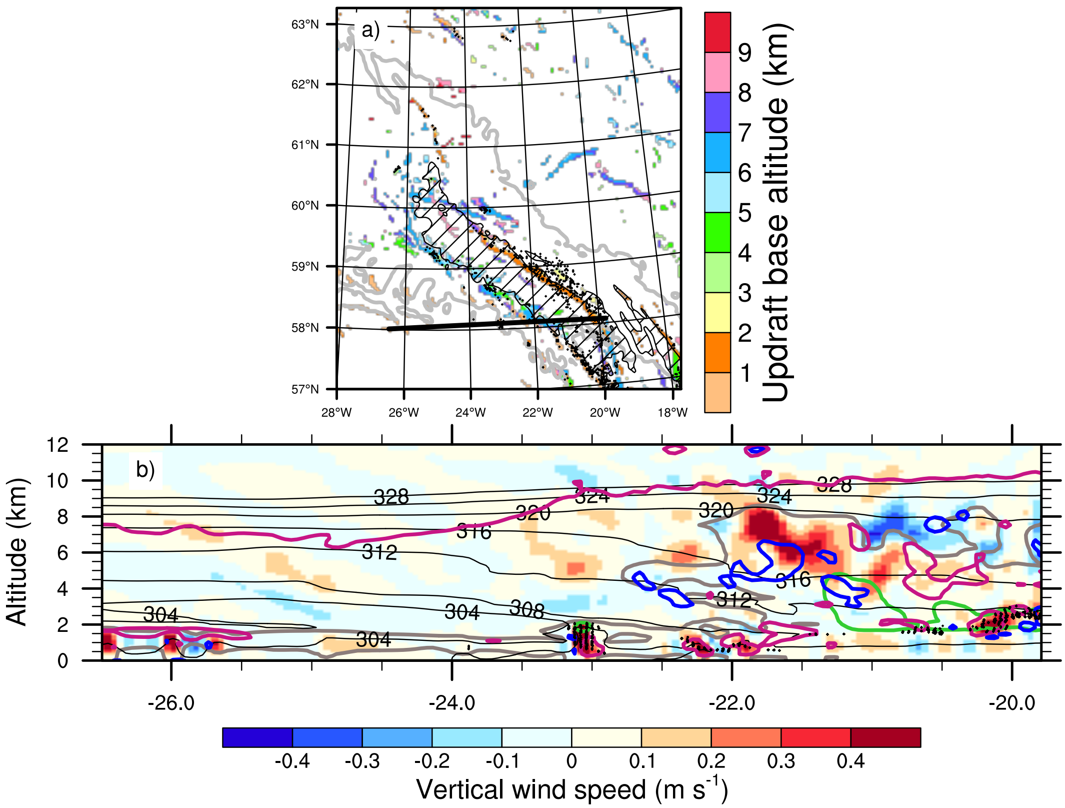

Figure 8. Simulation results at 15:00 UTC. (a) Base altitude of the connected grid points with a vertical wind speed greater than $0.3\,\mathrm{m\,s^{-1}}$ (shading, km). Grey contours and hatching show equivalent potential temperature (from 305 to 320 K every 5 K) and horizontal wind speed (values greater than $35\,\mathrm{m\,s^{-1}}$) at $1\,\mathrm{km}$ altitude, respectively. (b) Vertical wind speed (shading, $\mathrm{m\,s^{-1}}$) and equivalent potential temperature θ_e (black contours, every 4 K) along the black line shown in (a). ~~Double hatching shows horizontal wind speed greater than 35 below 2 altitude.~~ Grey ~~, light green~~ and light ~~blue~~ green contours show the cloud ~~, the graupel~~ and the ~~rain~~ graupel contents larger than $0.02\,\mathrm{g\,kg^{-1}}$, respectively. Magenta and navy blue contours show PV values equal to $2\,\mathrm{PVU}$ and $-1\,\mathrm{PVU}$, respectively. In (a) and (b), the black dots indicate the position of the rapid segments (one trajectory every 10 in (a)).

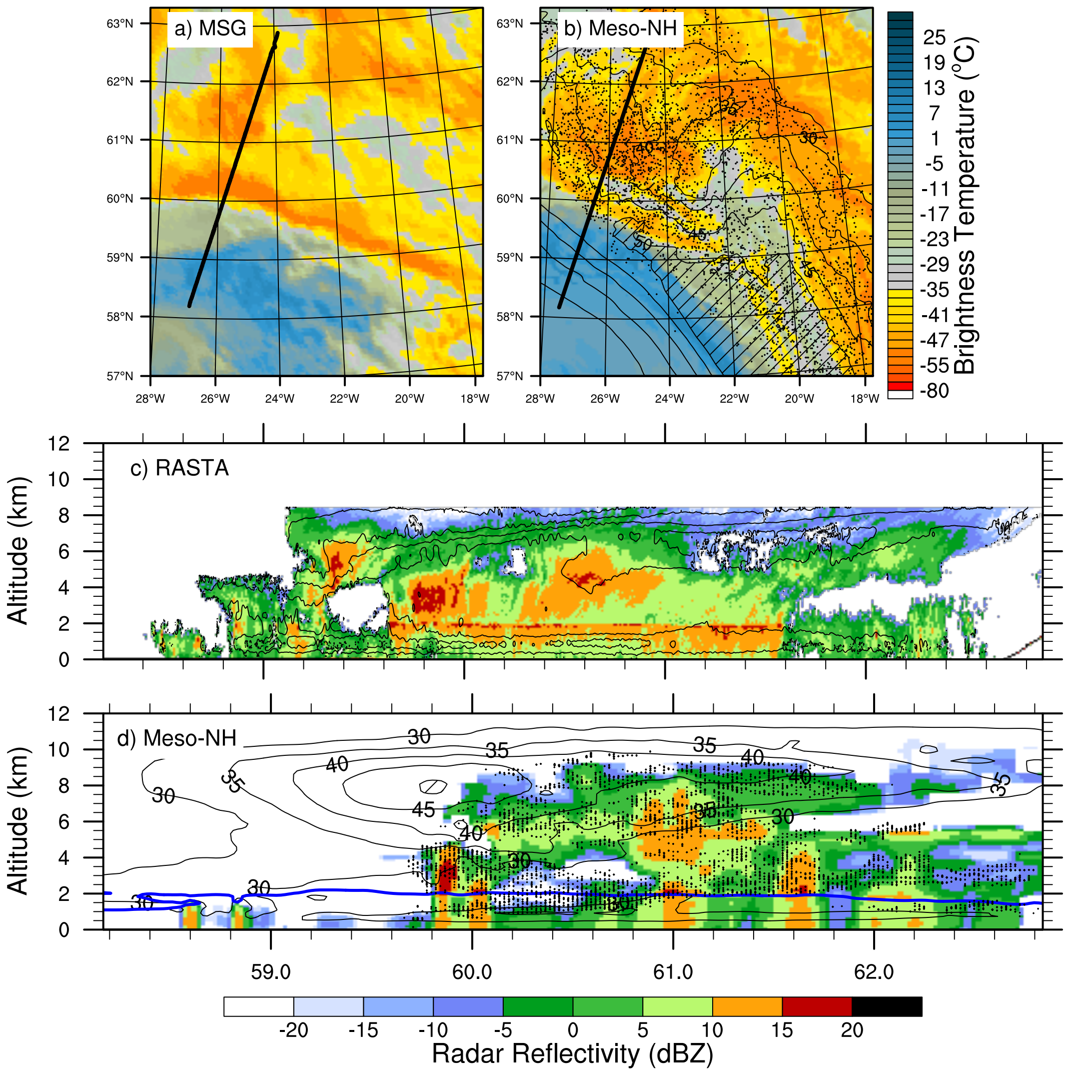

Figure 9. As in Fig. 7 but at 16:00 UTC.

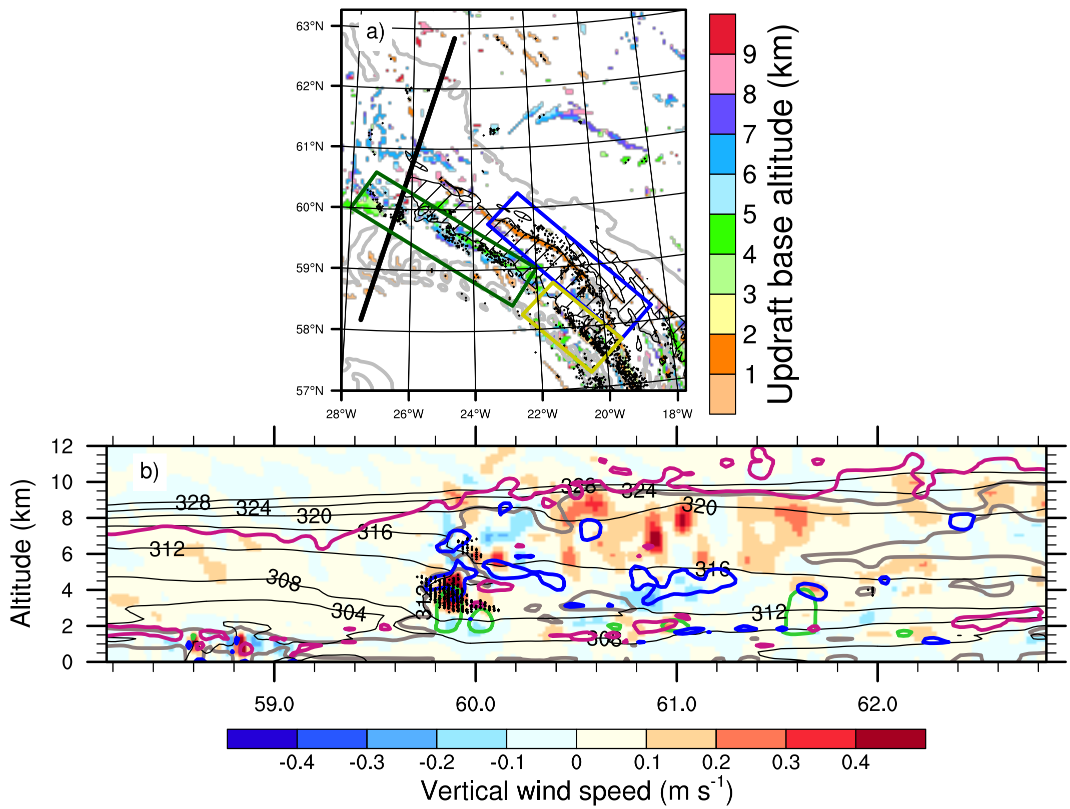

Figure 10. As in Fig. 8 but at 16:00 UTC. In (a), the dark green, yellow and blue boxes show where the three categories of fast ascents have been selected (see text).

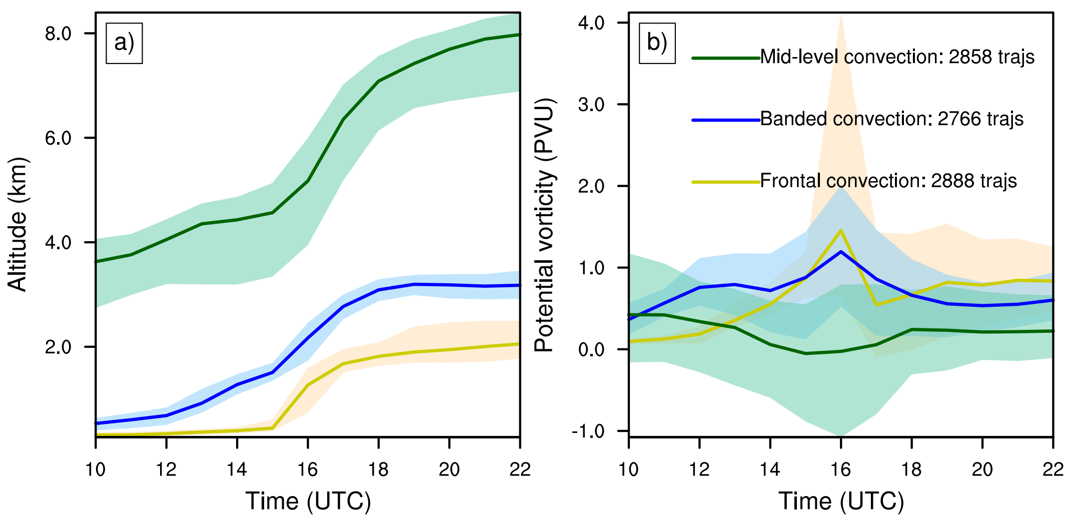

Figure 11. As in Fig. 6 but for (a) the altitude and (b) the PV of the frontal (in yellow), banded (in blue) and mid-level (~~cyclonic and anticyclonic~~ in green~~and orange, respectively~~) categories of convection.

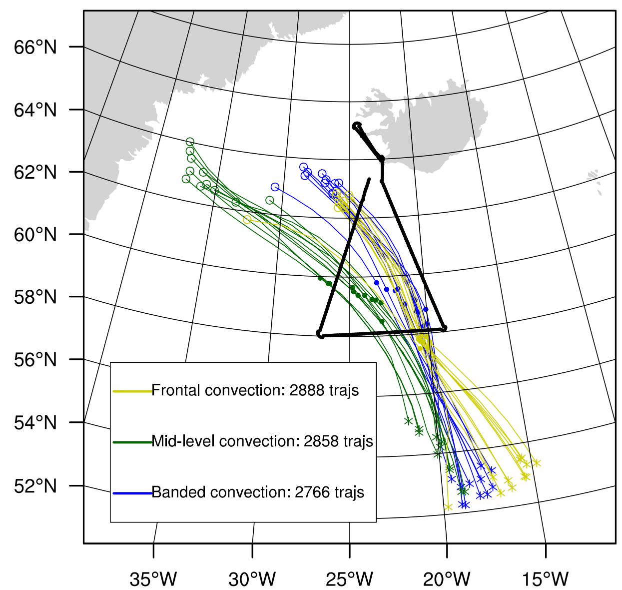

Figure 12. Trajectories of banded (in blue), frontal (in yellow) and mid-level (~~cyclonic and anticyclonic~~ in green~~and orange, respectively~~) convection between 10:00 and 22:00 UTC. Crosses, dots and circles show the location of the trajectories at 10:00, 16:00 and 22:00 UTC. Only ~~samples of~~ 10 ~~categories~~ samples are ~~plotted~~shown in each category.

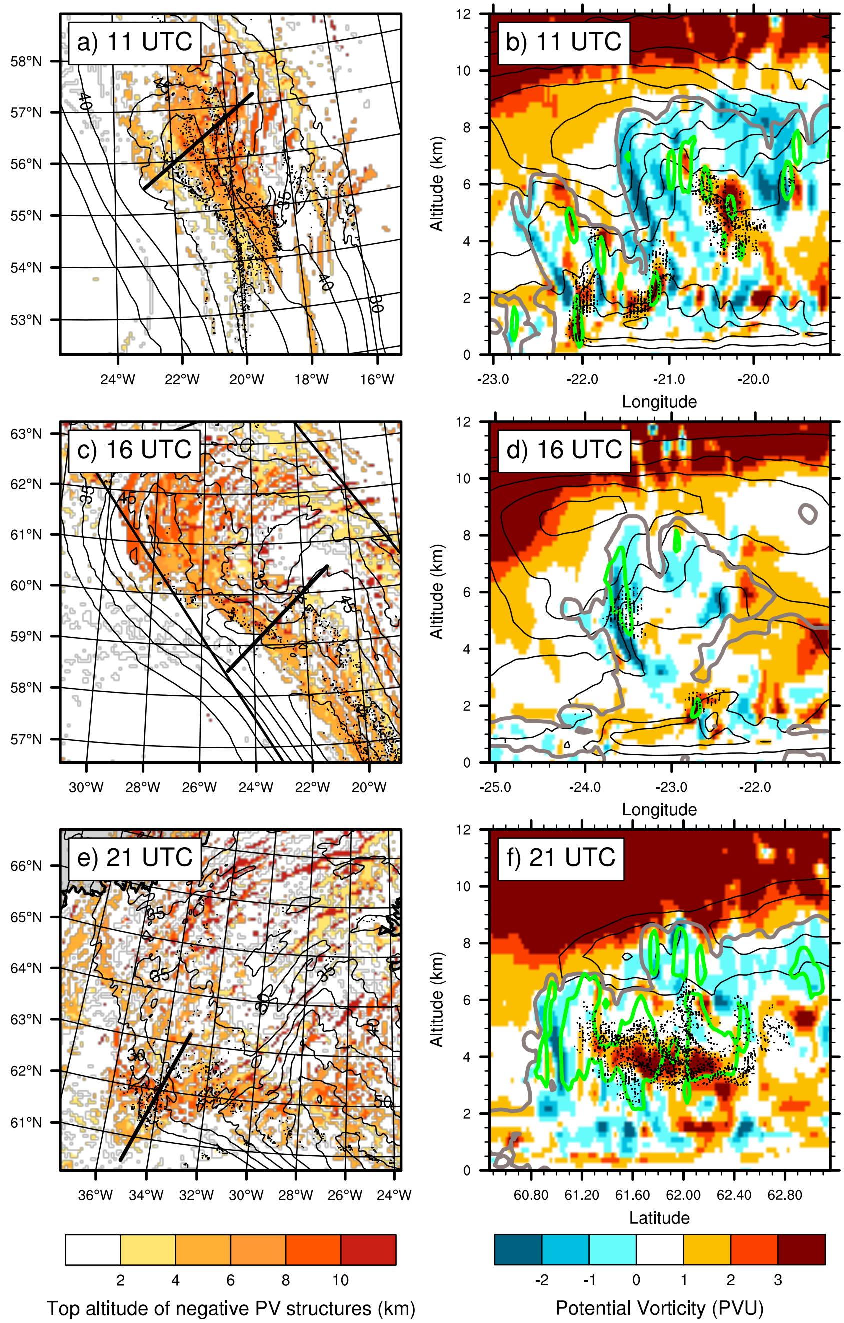

Figure 13. ~~Potential vorticity~~ PV at (a, b) 11:00 UTC, (c, d) 16:00 UTC and (e, f) 21:00 UTC in (a, c, e) maps of the top altitude of identified clusters below -1 PVU (shading, km) and (b, d, f) vertical cross-sections along the black thick line shown in (a, c, e), respectively. Dots indicate the position of rapid segments. ~~In~~ Black contours show horizontal wind speed (a, c, e) ~~, black contours show horizontal wind speed~~ at $\sim$9 km ~~altitude~~ and (b, d, f) in the cross-sections (values larges than 30 $\mathrm{m\,s^{-1}}$ every 5 $\mathrm{m\,s^{-1}}$). In (b, d, f) ~~black~~ green contours show ~~equivalent potential temperature (every 4) and blue contours shows~~ the vertical velocity equal to 0.3 $\mathrm{m\,s^{-1}}$.